IOP Publishing Quantum Sci. Technol. 9 (2024) 035048 https://doi.org/10.1088/2058-9565/ad4912

Quantum Science and Technology

OPEN ACCESS

RECEIVED
27 November 2023

REVISED
28 April 2024

ACCEPTED FOR PUBLICATION
9 May 2024

PUBLISHED
13 June 2024

PAPER

Mode analysis of spin field of thermal atomic ensembles

Weiyi Wang[1,2], **Mingming Xia**[2], **Wei Quan**[1,2,3] **and Kai Wei**[1,2,3,*]

[1] School of Instrumentation Science and Opto-electronics Engineering, Beihang University, Beijing 100191, People's Republic of China
[2] Hangzhou Innovation Institute, Beihang University, Hangzhou 310000, People's Republic of China
[3] Hefei National Laboratory, Hefei 230088, People's Republic of China
[*] Author to whom any correspondence should be addressed.

E-mail: weikai@buaa.edu.cn

Keywords: quantum gases, spin field, mode analysis, sensitivity limit, light-atom interaction

Abstract

The spin dynamics in a thermal atomic vapor cell have been investigated thoroughly over the past decades and have proven to be successful in quantum metrology and memory owing to their long coherent time and manipulation convenience. The existing mean field analysis of spin dynamics among the whole cell is sometimes inaccurate due to the non-uniformity of the ensemble and spatial coupling of multi-physical fields interacting with the ensembles. Here we perform mode analysis onto the quasi-continuous spin field including atomic thermal motion to derive Bloch mode equations and obtain corresponding analytical solutions in diffusion regime. We demonstrate that the widely used mean field dynamics of thermal gas is a particular case in our solution, corresponding to the uniform spatial mode. This mode analysis approach offers a precise method for analyzing the dynamics of the spin ensemble in greater detail from a field perspective, enabling the effective determination of spatially non-uniform multi-physical fields coupling with the spin ensembles, which cannot be accurately analyzed by the mean field method. Furthermore, this work paves the way to address quantum noises and relaxation mechanisms associated with non-uniform fields and inter-atomic interactions, which limit further improvement of ultra-sensitive spin-based sensors.

1. Introduction

Over the past few decades, thermal atomic ensembles have attracted significant attention across diverse fields, notably in quantum sensing [1], quantum metrology [2, 3], and quantum optics [4–6]. Relevant research includes mono-species alkali metal ensembles [7–9], hybrid alkali metal atomic ensembles [10–13], as well as hybrid atomic ensembles containing both alkali atoms and noble gases [14–16]. Despite substantial number of atoms, these atomic ensembles exhibit remarkable preservation of macroscopic coherence, even in the presence of numerous collisions [17–19]. This property has proven immensely beneficial for quantum precision measurements [20–25], new physics exploration [26–33], and the study of macroscopic quantum effects [34–37].

Most research has assumed a uniform spin distribution of atoms within atomic vapor cells, in other words, has relied on averaging method, which is a practical and reasonable approximation [38–40]. However, in actual situations, it is often inevitable to encounter spatially related non-uniform distributions. For instance, in hybrid atomic ensembles containing both alkali metal atoms and noble gas, the effective magnetic field (EMF) resulting from Fermi contact interactions is related to the polarization [41]. The polarization is non-uniform due to factors such as diffusion, light attenuation and transverse distribution, the probe region, and boundary conditions. Each atomic diffusion mode leads to specific unequal spin relaxation rate and spin polarization distribution. The pump light is inhomogeneous along its propagation direction through the cell due to strong absorption. Besides, it is also not uniform in the transverse plane perpendicular to the propagation direction [42], yet it is often treated as a function only dependent on the $\hat{z}$-direction with pumping rate $R_{\mathrm{op}}(z)$ [43]. Importantly, this observation has profound implications for quantum technologies, particularly in the realm of quantum sensing. The spatial variability in the pump

light and resultant atomic spin distributions challenge the assumptions underpinning current quantum sensing methodologies, potentially calling for a reevaluation of strategies to overcome spin projection noise through entanglement and squeezing. Furthermore, the probe light also has a transverse distribution. The measured atomic spin by the probe light corresponds to the region where the probe light energy is concentrated. This portion of atomic spin also exhibits spatial distribution with different modes, which requires evaluating the weight by the overlap between the light mode and the spin diffusion modes [36]. Magnetic field generated by coils is not perfectly uniform, which results in a spatially-related manipulation of atomic spins and spatially-related spin relaxation [44–46]. This nuanced understanding of spin dynamics could be pivotal in refining the operational parameters of quantum sensors, thereby enhancing their sensitivity and reliability. Other effects such as fluctuations in temperature lead to non-uniformity in the atomic number density distribution within the cell [24], highlighting the need for a more sophisticated analytical approach that accounts for the multi-physical field interactions within these systems. These process will influence the dynamics behavior both in spin evolution and properties of the quantum noise [36] and are sometimes difficult to evaluate due to the complex coupling among the facts above. The fundamental cause of these issues stems from the fact that the atomic vapor cell represents a macroscopic and multi-physical field system characterized by the presence of coupling effects among these physical fields. In situations where these non-local multi-physical interactions are non-negligible, such as ultra-sensitive measurement and inter-atomic correlation manipulation, the utilization of mean-field method for describing the atomic state within the vapor proves to be inadequately precise [19, 29, 47].

In this paper, we treat atomic spin ensemble as a physical quasi-continuous field with spatial distributions due to the dense atomic number and small volume of the cell. This methodology allows for a detailed examination of the spin ensemble dynamics, providing insights that are critical for the advancement of quantum sensing technologies. Firstly, we calculate the diffusion-corresponding orthonormalized eigenfunctions with three different boundary conditions in vapor cells of typical shapes. Secondly, employing the method of generalized Fourier expansion and combining the result with the obtained orthonormalized eigenfunctions, we derive the Bloch mode equations considering the diffusion term. This allows us to perform mode analysis on the described atomic spin fields and transform the problem of solving partial differential equations into solving a linear system of equations, whose solutions are the Fourier expansion coefficients of the field. We obtain an approximate 3D analytical solution for R_{op} in the case of collimation of pump light and diffusion relaxation rate much smaller than other relaxation rates, which is necessary for deriving Bloch mode equations in more detail. Through this approach, we uncover new avenues for optimizing the design and functionality of quantum sensors. Furthermore, we consider the transverse distribution of the probe light and define the overlap integral between the probe light mode and atomic diffusion modes to evaluate the contribution from each diffusion mode to the total signal. Finally, we derive steady-state analytical solutions for the longitudinal spin field and time-dependent analytical solutions for the transverse spin field. The spin average value relevant to the final output signal is calculated considering the actual measurement region, contrasting with the traditional approach of mean field method. As examples, we employ the solution to show concrete expression for alkali spin field in a cylindrical cell, relaxation rate considering diffusion, and transverse relaxation rate considering the gradient of the EMF induced by Fermi contact interaction. We also discuss the influence of the behavior of quantum noise under the consideration of atomic diffusion and multi-physics coupling.

The mode analysis method is particularly useful for quantum sensing based on thermal spin ensembles. The applications using thermal atomic vapor cell based on mean field method have realized several records for sensitivity such as ultra-sensitive atomic magnetometer [48], gradiometer [49], and new physics [50, 51]. However, further improvement of the ultrahigh sensitivity is limited by non-uniform multi-physical field noises, such as light inhomogeneity, magnetic field gradient, and EMF gradient. Our results indicate that, in comparison to mean-field methods, mode analysis approach provides a more accurate representation for the practical conditions within the ensemble of atomic spin field. Particularly, our model remains applicable in scenarios requiring the consideration of multi-physical field coupling. This precision is especially beneficial for capturing measurement signals more effectively, potentially leading to breakthroughs in quantum sensing technologies.

2. Method

Consider a thermal vapor cell with dense (typically $10^{12} \sim 10^{15}\mathrm{cm}^{-3}$ for alkali atoms and $10^{19} \sim 10^{20}\mathrm{cm}^{-3}$ for noble gas with nuclear spin $I = 1/2$) atoms constituting a spin field, $\boldsymbol{S} = \boldsymbol{S}(\boldsymbol{r}, t)$. Spin is equivalent to polarization with the definition $\boldsymbol{P}(\boldsymbol{r}, t) = \boldsymbol{S}(\boldsymbol{r}, t)/\langle \boldsymbol{S}(\boldsymbol{r}, t)\rangle$ and in the below the spin field refers to $\boldsymbol{P}(\boldsymbol{r}, t)$. We consider the thermal vapor cells in the Fickian diffusion regime, which the atomic motion is diffusive and could be modeled by the diffusion term $D\nabla^2\boldsymbol{P}$ [19]. Different from the Lagrange's view of particle movement

in fluid mechanics [36], we do not track on the dynamics of a single atom. This field is established by Euler's view of particle movement as in fluid mechanics. In other words, we focus on the spin dynamics in a small volume around position $\boldsymbol{r}$, ignoring the question of which atom provides the spin in this volume. The advantage of Euler's view is that it is suitable for describing macroscopic spin dynamics behavior, providing insights into the overall spin field dynamics. Besides, mathematically, this field is spatially differentiable. However, it cannot provide detailed information about an individual atom. In a number of sensing applications involving thermal atomic vapor cells, such as atomic magnetometer, co-magnetometer and spin gyroscope, the signal is obtained from a macro spin dynamics. Under these circumstances, more attention should be paid to the spin in the probe region rather than which atom provides the spin in this region, corresponding to Euler's view. To consider the micro effects such as quantum correlation, entanglement and random process modeling, it is better to use Lagrange's view.

Alkali-metal atoms and noble-gas atoms are most widely used thermal atomic ensembles, which are usually categorized as three types. The first kind is mono-species alkali atomic vapor cell, such as ^{87}Rb. The second kind is the hybrid alkali atomic vapor cell, such as ^{39}K and ^{87}Rb. The third kind is the hybrid alkali atomic vapor cell with noble gas, such as ^{39}K, ^{87}Rb and ^{3}He. The first two kinds are usually used in atomic magnetometer, especially for the spin-exchange-relaxation-free (SERF) magnetometer, reaching a fT/$\sqrt{\text{Hz}}$ sensitivity [21, 48]. The third kind is typically used in atomic co-magnetometer [50] and gyroscope [52] for seeking new physics such as dark matter [30]. The corresponding dynamic equations could be described by Bloch equations [53–55].

In general, the Bloch equations for the sth species kind of atomic ensemble considering diffusion term and its boundary condition [36] could be simply written as

$$\frac{\partial}{\partial t}\boldsymbol{P}_{\mathrm{s}} = i\left[\mathcal{H}_{\mathrm{s}}\left(\boldsymbol{r}\right), \boldsymbol{P}_{\mathrm{s}}\right] - \Gamma_{\mathrm{s},0}\boldsymbol{P}_{\mathrm{s}} + D_{\mathrm{s}}\nabla^2\boldsymbol{P}_{\mathrm{s}}, \tag{1}$$

$$\boldsymbol{P}_{\mathrm{s}}\left(\boldsymbol{r}\right) + \alpha_{\mathrm{s}}\left(\hat{\boldsymbol{n}}\cdot\nabla\right)\boldsymbol{P}_{\mathrm{s}}\left(\boldsymbol{r}\right) = 0, \boldsymbol{r}\in\Omega_{\mathrm{b}}, \tag{2}$$

where $\boldsymbol{P}_{\mathrm{s}} = \boldsymbol{P}_{\mathrm{s}}(\boldsymbol{r}, t)$ is the spin field of the s-th species kind of atomic ensemble at position $\boldsymbol{r}$ and time t. $\mathcal{H}_{\mathrm{s}}(\boldsymbol{r})$ is the Hamiltonian of the s-th species kind of atomic ensemble considering the ground state interactions, such as Zeeman effects and hyperfine interactions, spin–spin interactions such as spin-exchange collisions and light-atom interactions such as light-shifts at position $\boldsymbol{r}$. $\Gamma_{\mathrm{s},0}$ is the relaxation rate of the s-th species kind of atomic ensemble without diffusion induced relaxation and gradient relaxation rate in the interaction Hamiltonian term, such as relaxation rate induced by magnetic field gradient. D_{s} is the diffusion coefficient of the s-th species kind of atomic ensemble. $\alpha_{\mathrm{s}} = \frac{2}{3}\frac{1+e^{-1/N_{\mathrm{s}}}}{1-e^{-1/N_{\mathrm{s}}}}\bar{\lambda}$ is the parameter describing the boundary for the cell with N_{s} being the average number of wall collisions that the spin withstands before depolarizing [56] and $\bar{\lambda} = \frac{3D_{\mathrm{s}}}{2\bar{v}}$ is the mean free path of the atoms, where $\bar{v}$ being the thermal velocity. $\hat{\boldsymbol{n}}$ is the outward normal unit vector at the boundary. Ω_{b} is the boundary of the cell in geometry. When $N_{\mathrm{s}}\sim 1$, i.e. the s-th species kind of atomic ensemble inside the cell rapidly depolarize through first wall collisions, we have $\alpha_{\mathrm{s}}\approx 0$, the boundary condition equation (2) becomes Dirichlet boundary condition $\boldsymbol{P}_{\mathrm{s}} = 0$ corresponding to the ideal uncoated vapor cell. When $N_{\mathrm{s}}\sim\infty$, i.e. the s-th species kind of atomic ensemble inside the cell never depolarize through wall collisions, we have $\frac{1}{\alpha_{\mathrm{s}}}\approx 0$, the boundary condition equation (2) becomes Neumann boundary condition $\left(\hat{\boldsymbol{n}}\cdot\nabla\right)\boldsymbol{P}_{\mathrm{s}} = 0$ corresponding to the ideal coated vapor cell or noble gas with stable shielding structures. The practical condition in the experiments is the middle occasion when α_{s} is a finite number as equation (2), which leads to Robin boundary condition corresponding to the non-ideal coated vapor cell. We demonstrate the explicit form of Bloch equations satisfying equations (1) and (2) for the three kinds of ensembles including one species of alkali atomic ensemble, hybrid alkali atomic ensemble and hybrid alkali atomic vapor cell with noble gas in appendix A. We use all the eigenfunctions $\{u_{\mathrm{s},n}(\boldsymbol{r})\}$ of the Helmholtz equation $\nabla^2 u_{\mathrm{s},i}(\boldsymbol{r}) + k_{\mathrm{s},i}^2 u_{\mathrm{s},i}(\boldsymbol{r}) = 0, i = 1, 2, \ldots$ to expand the spin field of s-th species kind of atomic ensemble. By performing the Fourier integral to obtain mode equations for expansion coefficients, we combine the equations for the ensemble containing all the species. These coefficient equations can then be written in a simpler form which we call them *Bloch mode equations*

$$\mathcal{A}\mathcal{P}_z = \mathcal{R}, \tag{3}$$

$$\frac{\mathrm{d}}{\mathrm{d}t}\mathcal{P}_+ = \left(i\Omega - \mathcal{A}\right)\mathcal{P}_+ - i\Omega_+\mathcal{P}_z, \tag{4}$$

with the definition of coefficient matrix in appendix A. For mono-species ensemble, $\mathcal{P}_z$ and $\mathcal{P}_+$ are the arrays composed by expansion coefficients. The i-th eigenvalue of $i\Omega - \mathcal{A}$ is a complex number whose absolute value of the real part is the relaxation rate and the imaginary part is the Lamor precession frequency for the i-th mode. Ω_+ is related to the transverse magnetic field. For multi-species atomic ensemble, same form could be derived by combining the related expansion coefficients to an extended array and the

coefficient matrix into block matrices as shown in appendix A. At this stage, we can directly solve the expansion coefficient array under the condition of a modulated transverse magnetic field $\Omega_+(t) = \tilde{\Omega}_+ e^{i\omega t}$

$$\mathcal{P}_z = \mathcal{A}^{-1}\mathcal{R}, \tag{5}$$

$$\mathcal{P}_+(t) = \left[-\omega\mathcal{I} + \Omega + i\mathcal{A}\right]^{-1}\Omega_+(t)\mathcal{P}_z. \tag{6}$$

After obtaining the expansion coefficients, one can recover the spin field with the definition of Fourier expansion

$$P_{\mathrm{s},z}(\boldsymbol{r}) = \mathcal{P}_{\mathrm{s},z}^T \mathcal{U}_\mathrm{s}(\boldsymbol{r}), \tag{7}$$

$$P_{\mathrm{s},+}(\boldsymbol{r},t) = \mathcal{P}_{\mathrm{s},+}^T(t)\mathcal{U}_\mathrm{s}(\boldsymbol{r}), \tag{8}$$

where $\mathcal{U}_\mathrm{s}(\boldsymbol{r}) = [u_{\mathrm{s},1}(\boldsymbol{r}), u_{\mathrm{s},2}(\boldsymbol{r}), \ldots u_{\mathrm{s},n}(\boldsymbol{r}), \ldots]^T$ is the 1-D array composed by the eigenfunction of the sth atomic ensemble.

Specially, to the simplest case when there is only one species kind of alkali atomic ensemble and all the field has only one uniform diffusion mode with the same eigenfunction $u = \frac{1}{\sqrt{V}}$, as shown in appendix A, $\mathcal{A}$ is simplified to $\frac{R_\mathrm{tot}}{Q} = \frac{R_\mathrm{rel}+R_\mathrm{op}}{Q} + Dk^2$ with k being the wave number of the uniform mode and Dk^2 is the diffusion relaxation rate of the uniform mode, Ω is simplified to $\omega_0 = \frac{\gamma_e B_0}{Q}$ and $\Omega_+ = \frac{\gamma_e B_+}{Q}$, $\mathcal{R} = \int R_\mathrm{op}\frac{1}{\sqrt{V}}\mathrm{d}V = \sqrt{V}R_\mathrm{op}$. By assuming the transverse magnetic field $B_+ = \tilde{B}_+ e^{i\omega t}$, we obtain in this case

$$P_{\mathrm{e},z} = \frac{R_\mathrm{op}}{R_\mathrm{tot}}, \tag{9}$$

$$P_{\mathrm{e},+}(t) = -\frac{i\gamma_e \tilde{B}_+ P_{\mathrm{e},z}}{Q}\frac{1}{\frac{R_\mathrm{tot}}{Q} + i(\omega - \omega_0)}e^{i\omega t}, \tag{10}$$

which is a common result for mean field method in alkali atomic magnetometer [53] where we have chosen the subscript s = e in equations (7) and (8) for electronic spin of a single species atomic ensemble. This verification is the same for other atomic ensembles mentioned above. In this way we conclude that the mean field method is a special case in our method with uniform distribution mode.

Most research regards pumping rate $\bar{R}_\mathrm{op}$ as the average value though there is always absorption in light, which is a practical approximation for mean field method. However, when we perform mode analysis, pumping rate could be regarded as a spatial function $R_\mathrm{op} = R_\mathrm{op}(\boldsymbol{r})$. This means it is still not sure when determining the coefficient matrix such as $\mathcal{R}$ combined by the pumping rate of each order since this makes the pumping term nonlinear when performing Fourier integral. Thus, in appendix B we have calculated $R_\mathrm{op}(\boldsymbol{r})$ for several common cases. The pumping rate $R_\mathrm{op}(\boldsymbol{r})$ in a cylindrical vapor with the incident light propagating along the axial direction is given by

$$R_\mathrm{op}(\rho, z) = R_\mathrm{rel} W\left(A(\rho)e^{-n\sigma(\nu_0)z + A(\rho)}\right), \tag{11}$$

where

$$A(\rho) = \frac{R_\mathrm{op}(\rho, 0)}{R_\mathrm{rel}}. \tag{12}$$

To demonstrate the validity of the approximation that the transverse distribution remains unchanged during the propagation of the light, we compare the numerical solution results with this result. The reliability of the results is verified for various common experimental parameter scenarios when diffusion effect is negligible. According to equation (11), at a fixed relaxation rate $R_\mathrm{rel} = 400\ \mathrm{s}^{-1}$, we assume the transverse distribution is $R_\mathrm{op}(\rho, 0) = R_\mathrm{op}(0)e^{-\frac{2\rho^2}{w_0^2}}$ and simulate the analytical solution at different pump beam waist radii w_0, various pump-to-relaxation rate ratios $R_\mathrm{op}/R_\mathrm{rel}$, and different absorption coefficients $n\sigma$ in a cylindrical vapor cell with length $L = 1.2$ cm and $R = 0.6$ cm, obtaining the result as shown in figure 1.

We have so far obtained the dynamics of the spin field under the consideration of pump light with absorption in propagating direction, transverse distribution and diffusion of the atoms. However, in some cases involving two beams that one of them is resonant which is used for pumping and the other one, whose radius is usually small, has a large detuning and little absorption which is used for probing, one should consider the overlap between the probe light modes and the atomic ensemble diffusion modes since only the

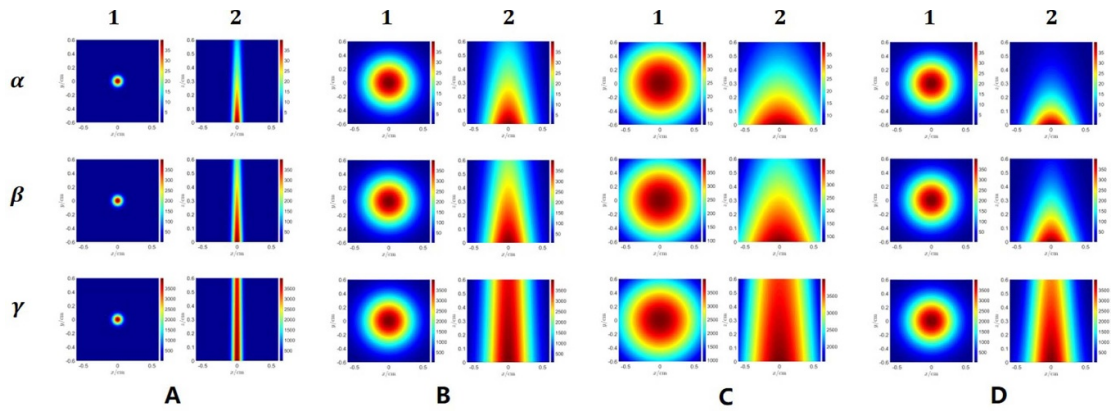

Figure 1. Simulation of $R_{\mathrm{op}}(\rho, z)$ according to equation (11) at different parameters. The length of the cell is 1.2 cm. (A) $w_0 = 0.1$ cm, $n\sigma = 2\ \mathrm{cm}^{-1}$.(B) $w_0 = 0.5$ cm, $n\sigma = 2\ \mathrm{cm}^{-1}$. (C) $w_0 = 1.0$ cm, $n\sigma = 2\ \mathrm{cm}^{-1}$. (D) $w_0 = 0.5$ cm, $n\sigma = 5\ \mathrm{cm}^{-1}$. The α line is the case for $R_{\mathrm{op}} = 0.1R_{\mathrm{rel}}$. The β line is the case for $R_{\mathrm{op}} = R_{\mathrm{rel}}$. The γ line is the case for $R_{\mathrm{op}} = 10R_{\mathrm{rel}}$. Column 1 corresponds to the results for the cross-section at $z = 0$, and Column 2 corresponds to the results for the cross-section at $y = 0$.

overlap region is effective in measurement [36]. The calculation detail for this fact is trivial and we have attached it in appendix C. Here, we only show that the final measured signal is given by

$$I_m(t) \propto \bar{P}_{\mathrm{s},+m}(t) = \frac{1}{\tau}\int_0^{\tau}\left[\frac{1}{V}\int_V P_{\mathrm{s},+m}(\boldsymbol{r}, t)\,\mathrm{d}V\right]\mathrm{d}t. \tag{13}$$

V is the volume of the cell and τ is measuring time. $P_{\mathrm{s},+m}(\boldsymbol{r}, t)$ is the transverse polarization of $P_{s,+}(\boldsymbol{r}, t)$ measured by the probe light with specific mode at position r and time t. This is the general expression for the measured signal considering diffusion effects. It could help to design the optimal parameters to obtain better responses as a target function. In this way, we can evaluate the contribution of each segment of the atomic ensemble within the cell to the final signal. Employing an effective detection radius to assess the effective detection volume is a simple and useful approximation during this evaluation [43]. However, in this approximation, the judicious selection of the effective detection radius becomes particularly crucial and sometimes ambiguous. By utilizing our model, these difficulties can be circumvented, as the atoms within the cell can interact with the light by evanescent field whose contribution is relatively small, making the volume of integration in equation (C4) equal to the volume of the whole cell.

The Lamor precession frequency and relaxation rate of spin ensembles are two vital observable quantity in a thermal atomic vapor cell since they reflect the quantum state of the atomic ensemble. The dynamic response of the system is determined once these two parameters are determined. In the past, these two parameters are usually regarded as constants having no connection with space. However, upon careful consideration, the Lamor precession frequency and relaxation rate vary across different position due to spatial coupling effects such as the motion of the atoms, the distribution of the light, and the gradient of the magnetic field. Here, we demonstrate that our model could analyze the spatial distribution of the Lamor precession frequency and relaxation rate by every order of the mode.

To obtain the relaxation rate, we calculate the eigenvalue of equations (3) and (4). First, we consider the longitude relaxation rate. This relaxation rate is the real part of the eigenvalue given by equation (3)

$$\left|\mathcal{A} - \tilde{\lambda}_1\mathcal{I}\right| = 0. \tag{14}$$

Thus, the longitude diffusion relaxation rate for the ith mode is $\frac{1}{T_1^{(i)}} = \mathrm{Re}[\tilde{\lambda}_{1,i}]$. If the pumping rate $R_{\mathrm{op}}(\boldsymbol{r})$ is spatially uniform, then $\mathcal{A}$ is a diagonal matrix and the diagonal element is the eigenvalue. For transverse relaxation rate, the eigenvalue of equation (4) is given by

$$\left|(i\Omega - \mathcal{A}) - \tilde{\lambda}_2\mathcal{I}\right| = 0, \tag{15}$$

In general, $\tilde{\lambda}_{2,i} = i\omega_i - \frac{1}{T_{2,i}}$ is a complex number whose real part is the opposite number of relaxation rate and imaginary part is Lamor precession frequency of the ith mode [18]. Similarly, we obtain transverse relaxation rate for the ith mode $\frac{1}{T_2^{(i)}} = -\mathrm{Re}[\tilde{\lambda}_{2,i}]$ and the Lamor precession frequency of the ith order is the imaginary part of the eigenvalue given by $\omega_i = \mathrm{Im}[\tilde{\lambda}_{2,i}]$. At this stage, we conclude that the Lamor precession

and relaxation rate frequency are given by the coefficient matrix of the mode equations. This result could help us to consider some polarization-related relaxation such as EMF gradient induced by Fermi contact interaction in hybrid atomic vapor cell involving alkali atoms and noble gas.

We end this section by summarizing the eigenfunctions for Helmholtz equation at 3 kinds of classical boundary conditions, i.e. Dirichlet boundary condition (D-BC), Neumann boundary condition (N-BC), and Robin boundary condition (R-BC) for 3 kinds of common shapes of vapor cells, i.e. rectangular, cylindrical and spherical with their normalization coefficients as shown in table 2.

3. Applications and examples

We will illustrate the applications of the aforementioned model above with specific examples to demonstrate its practical application value and potential scenarios. This includes calculating the field distribution of alkali metal atomic spin polarization, the relaxation rate considering diffusion process within a given axisymmetric cylindrical cell under D-BC, and the transverse relaxation rate considering EMF gradient generated by Fermi contact interactions.

3.1. Spin field distribution of Rb in a cylindrical vapor cell

The eigenfunctions given by Helmhotz equation of an axisymmetric cylindrical cell possess characteristics of both the rectangular cell and the spherical cell, making them versatile for demonstration. Here, we consider such a cell without coating. In the absence of coating, alkali metal atoms inside the cell rapidly depolarize through first wall collisions, corresponding to D-BC as N tends to 1. According to table 2, under axisymmetric condition $n=0$ since the different orders of the Bessel function J_n correspond to different radial modes, and in axisymmetric situations, only the fundamental radial mode ($n=0$) maintains symmetry, and similarly we have $m=0$. Thus, the eigenfunctions of D-BC in this case are

$$u_{\nu l}(\rho,z)=\sqrt{\frac{2}{\pi LR^2}}\frac{J_0(k_\nu\rho)}{|J_1(k_\nu R)|}\sin\left(\frac{l\pi}{L}z\right), \tag{16}$$

where k_ν is the ν-th eigenvalue for zero order Bessel function satisfying $J_0(k_\nu R)=0$. Specifically, we consider a cylindrical ^{87}Rb atomic cell with parameters shown in table 1. We have obtained the spin field distribution P_{ez} of ^{87}Rb as shown in figure 2 with cutoff order for Bessel function $n=4$ and for z-mode $m=40$ to make sure the overlap integral has been convergent.

At the boundary the spin is zero corresponding to our assumption of D-BC and we can clearly see the distribution in both $\hat{\boldsymbol{z}}$-direction and $\hat{\boldsymbol{\rho}}$-direction. Besides, the maximum polarization is $0.48\lesssim 0.5=\frac{R_{\rm op}}{R_{\rm op}+R_{\rm rel}}$ since we ignore the diffusion induced relaxation rate in the light to an approximation but we consider it in the atomic ensemble and the total relaxation rate is $R_{\rm tot}=R_{\rm rel}+R_{\rm diff}$ where $R_{\rm diff}$ is the relaxation rate induced by diffusion.

Now assume that we have another probe light propagating along x-axis. In experiment, measured $P_{s,+}$ could be obtained according to equation (C4). However, under this circumstance, we need to consider the flattened overlap integral matrix $\mathcal{H}_{nm\times nm}$ defined in equation (C3) with extended index whose matrix element is

$$h_{\nu l\mu k}=\int_0^L \mathrm{d}z\int_0^{2\pi}\mathrm{d}\phi\int_0^R \rho\mathrm{d}\rho e^{-\frac{2\rho^2}{w_0^2}}u_{\nu l}(\boldsymbol{r})\,u_{\mu k}(\boldsymbol{r}). \tag{17}$$

Additionally, as shown in figure 3, one could substitute the transverse distribution function of the probe light with a bimodal Gaussian function, denoted as $f_{BG}(x,y)=C_f(e^{-2\frac{(x-x_0)^2+y^2}{w_0^2}}+e^{-2\frac{(x+x_0)^2+y^2}{w_0^2}})$, to determine the optimal distance for differential measurement in magnetometer with two parallel detection beams or space correlation analysis between the two beams due to diffusion effect. The normalization coefficient C_f of general transverse mode could be obtained by $\int_V f(\boldsymbol{r})\mathrm{d}^3\boldsymbol{r}=1$.

3.2. Relaxation rate considering diffusion effects

In the case of mean field method, the relaxation rate induced by diffusion is an inevitable and limiting factor for precision measurement. Due to the diffusion of the atoms, the imperfection of the transverse distribution of the light and other multi-physics coupling effects, the relaxation rate is non-uniform since each diffusion mode is related to its own preferred region and specific mode relaxation rate. Here, we show an example in a cylindrical Rb^{87} atomic vapor cell with D-BC. For simplicity, we assume that the length of the cell is much longer than the radius $L\gg R$ and azimuth symmetry, which means that the eigenfunction is

$$u_\nu(\rho)=\sqrt{\frac{1}{\pi LR^2}}\frac{J_0(k_\nu\rho)}{|J_1(k_\nu R)|}, \tag{18}$$

Table 1. Simulation parameters for cylindrical ^{87}Rb atomic cell.

Symbol	Meaning	Value/Expression
L	Cell length	0.6 cm
R	Cell radius	0.3 cm
T	Cell temperature	393.15 K
p_{N_2}	Pressure of N_2	500 Torr
w_0	Pumping light radius	0.3 cm
R_{rel}	Relaxation rate excluding diffusion	400 s^{-1}
n_{Rb}	Atomic density for ^{87}Rb	$\frac{1}{T[1/K]} 10^{21.866+A-B/T}$ cm^{-3}
A	Parameter for n_{Rb}	4.312
B	Parameter for n_{Rb}	4040 K
Q	Slowing down factor	5.5
$R_{op}(0)$	Pumping rate at $z = 0$	400 s^{-1}
σ	Absorption section of ^{87}Rb	1.8×10^{-13} cm^2

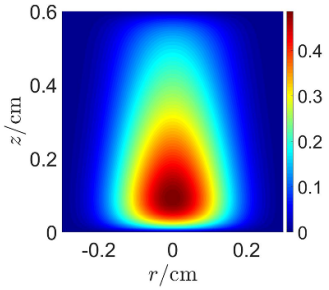

Figure 2. Calculated spin field distribution of $P_{ez}(\boldsymbol{r})$ of ^{87}Rb by D-BC. Simulation parameters are shown in table 1 .

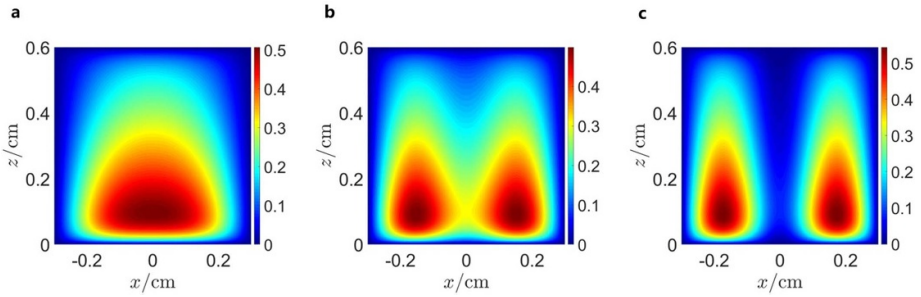

Figure 3. Polarization distribution of two beams of Gaussian pump light in $y = 0$ plane. The distance between the two beams are $2x_0 =$ (**a**) 0.2 cm, (**b**) 0.3 cm, (**c**) 0.4 cm corresponding to different coupling strength due to diffusion. Other simulation parameters are the same as figure 2.

where the normalization coefficient in table 2. is $A_{n\nu lm} = A_{n\nu}A_lA_m$ with $A_{n\nu} = A_\nu = \sqrt{2}/R|J_1(k_\nu R)|$ due to azimuth symmetry, $A_l = \sqrt{1/L}$ and $A_m = \sqrt{1/2\pi}$ due to uniform distribution.

The dynamics of the spin field is shown in appendix A equations (A4) and (A5). Here we consider a ^{87}Rb atomic cell with a length of $L = 5$ cm and a radius of $R = 0.3$ cm. The cell is so long since it is beneficial for enhancing light-atom interactions in some quantum entanglement experiments [37]. Other conditions are the same as 3.1 while we choose average longitude pumping rate with transverse distribution $\tilde{R}_{op} = 400\frac{2}{\sqrt{\pi L w_0^2}} e^{-2\rho^2/w_0^2}$ s^{-1} so that the νth order pumping rate is given by $R_{op}^{(\nu)} = \int_V \tilde{R}_{op}(x,y)u_\nu dV$. In this case, we have

$$\mathcal{A}_{ij} = c_{ij} + \left(\frac{R_{rel}}{Q} + D_e k_\nu^2\right)\delta_{ij}, \tag{19}$$

$$\Omega_{ij} = \omega_0 \delta_{ij}. \tag{20}$$

Calculating the eigenvalue, we find the relaxation rate for each mode. To intuitively show the mode relaxation rate, we display first 6 diffusion eigenmodes as shown in figure 4, which demonstrates that the

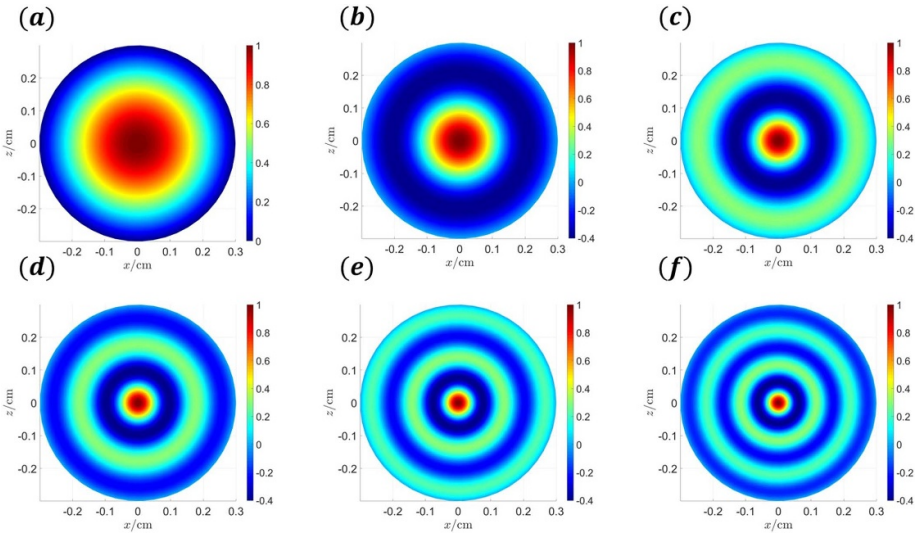

Figure 4. First 6 normalized eigenmodes of diffusion process in the cylindrical ^{87}Rb atomic cell in transverse plane. The color stands for the normalized amplitude at corresponding position. Corresponding transverse relaxation rate is (**a**) $\frac{1}{T_{2,0}} = 200.18\ \mathrm{s}^{-1}$, (**b**) $\frac{1}{T_{2,1}} = 267.43\ \mathrm{s}^{-1}$, (**c**) $\frac{1}{T_{2,2}} = 340.76\ \mathrm{s}^{-1}$, (**d**) $\frac{1}{T_{2,3}} = 452.85\ \mathrm{s}^{-1}$, (**e**) $\frac{1}{T_{2,4}} = 602.16\ \mathrm{s}^{-1}$, (**f**) $\frac{1}{T_{2,5}} = 787.42\ \mathrm{s}^{-1}$. The length of the cell is $L = 5$ cm and the radius is $R = 0.3$ cm. The radius of the pumping light beam is $w_0 = 0.3$ cm. Other conditions are the same as figure 2.

relaxation rate for each mode indeed has a preferred area. When the atoms are in diffusion regime, multiple modes can be stimulated, each contributing to the total field with a specific relaxation rate.

The mode relaxation rates become larger with the increase of the order. This is similar to electromagnetic field in a fiber, the higher order mode usually has a higher damping rate since it has a larger attenuation section in the $\hat{\boldsymbol{\rho}}$-direction. To obtain a narrower linewidth, the fundamental mode is needed. That means we should use a probe light that has more overlap with the fundamental mode and less overlap with other higher order modes. This could be realized either by the design of the geometry shape of the cell or by adjusting the radius and transverse distribution of the probe beam. One more interesting thing is the manipulation of the higher order modes. The relaxation rate is large for higher order modes which means it may have a broader bandwidth than fundamental modes. The simplest way to simulate higher order modes is to find the corresponding transverse distribution of the probe light to achieve the largest overlap integral between the mode of probe light and the higher order modes of the spin field so that a higher coupling efficiency would be obtained.

3.3. Transverse relaxation rate induced by EMF

In the following discussion, we consider the vapor cell filled with hybrid alkali atomic vapor denoted by e and noble gas denoted by n. The gradient of the magnetic field is a primary factor influencing the relaxation rate of the spin field in hybrid atomic ensemble including noble gas [57]. Previous research has focused on the effects of classical magnetic field gradients and their suppression methods [29]. However, in hybrid alkali-noble gas ensemble, an EMF gradient introduced by Fermi contact becomes significant and, in some cases, even the predominant factor [11]. Nevertheless, research on this pseudomagnetic field gradient is extremely limited. The mode analysis proposed in this paper offers a novel approach for its study and suppression.

The gradient of magnetic field will lead to additional relaxation process and the corresponding relaxation rate of normal magnetic field in spherical vapor cell has been analyzed in [29]. However, the magnetic field experienced by alkali atoms is $\boldsymbol{B}(\boldsymbol{r}) + \lambda M_n \boldsymbol{P}^n(\boldsymbol{r})$ and the magnetic field experienced by noble gas is $\boldsymbol{B}(\boldsymbol{r}) + \lambda M_e \boldsymbol{P}^e(\boldsymbol{r})$ where the second term is due to Fermi contact interaction between alkali atoms and noble gas. Thus, it is not only of interest but also essential to analyze the relaxation rate generated by the pseudomagnetic field gradient $\lambda M_n \nabla \boldsymbol{P}^n(\boldsymbol{r})$ and $\lambda M_e \nabla \boldsymbol{P}^e(\boldsymbol{r})$ as well in some research involving precision measurement. Strictly, λ is dependent on the shape of the cell and the position which should be evaluated by using the technique of scalar magnetic potential [58]. Nevertheless, the uncertainty influenced by λ in the measured region leads to errors on the order of $1\% \sim 2\%$ which can be corrected by a shape factor $C(\boldsymbol{r})$ defined in (8) of [44]. We have assumed that this factor is a constant $C = 8\pi/3$ for a uniformly magnetized sphere or a cube, $C = 4\pi$ for a very long cylinder with a uniform magnetization parallel to its axis, or $C = 2\pi$ for a cylinder magnetized perpendicular to its axis. Under this assumption, in our method, the gradient

operator ∇ only operates on eigenfunctions since we have separated the variables by Fourier expansion. According to equations (7) and (8), the corresponding gradient of eigenfunctions are related to eigenvalues,

$$\nabla P_{\mathrm{a},\alpha}(\boldsymbol{r}) = \sum_{i=1}^{n} P_{\mathrm{a},\alpha}^{(i)} \nabla u_{\mathrm{a}}^{(i)}(\boldsymbol{r}), \quad \mathrm{a} = \mathrm{e},\mathrm{n}, \quad \alpha = x,y,z. \tag{21}$$

In this way, we obtain the gradient of EMF induced by Fermi contact interaction $\nabla B_{\mathrm{a},\alpha}(\boldsymbol{r}) = \lambda M_{\mathrm{a}} \nabla P_{\mathrm{a},\alpha}(\boldsymbol{r})$. The gradient of eigenfunctions is simple to calculate since these functions are all primary functions, which enables us to design gradient coils. One ideal method is to design the gradient magnetic field according to the eigenfunctions of diffusion. However, we have to point out that in some cases this may not be realistic since the order of expansion modes are quite high especially in the $\hat{\boldsymbol{z}}$-direction and further analysis is needed. This design is more effective when the expansion order is low.

To emphasize the relaxation rate generated by the EMF gradient, we assume that the classical magnetic field is spatially uniform. In other words, there is no relaxation rate generated by the gradient of the ordinary magnetic field. We consider the vapor cell with D-BC for alkali atoms and N-BC for noble gas with a 2D azimuth symmetry case, so that according to table 2, the eigenfunctions for alkali atoms and noble gas are

$$u_{\mathrm{e},\nu}(\rho) = \sqrt{\frac{1}{\pi L R^2}} \frac{J_0(k_{\mathrm{e},\nu}\rho)}{|J_1(k_{\mathrm{e},\nu}R)|}, \tag{22}$$

$$u_{\mathrm{n},\mu}(\rho) = \sqrt{\frac{1}{\pi L R^2}} \frac{J_0(k_{\mathrm{n},\mu}\rho)}{|J_0(k_{\mathrm{n},\mu}R)|}, \tag{23}$$

where $k_{\mathrm{e},\nu}$ is the νth eigenvalue for the electron spin in D-BC and $k_{\mathrm{n},\mu}$ is the νth eigenvalue for the noble gas spin in N-BC. According to equation (6), when the EMF is nonuniform, the eigenvalue equation is the given by equation (15) and eigenvalue $\tilde{\lambda}_2 = i\tilde{\omega} - \frac{1}{T_{2,n}}$ is a complex number whose opposite number of real part is the relaxation rate of the corresponding mode and the imaginary part stands for the effective Lamor precession frequency. Thus, the transverse relaxation rate for the ith mode of alkali atoms and jth mode of noble gas atoms added by the Fermi contact interaction gradient is given by $\frac{1}{T_{2,\mathrm{e}}^{(i)}} = -\mathrm{Re}[\tilde{\lambda}_{2,\mathrm{e}i}]$ and $\frac{1}{T_{2,\mathrm{n}}^{(j)}} = -\mathrm{Re}[\tilde{\lambda}_{2,\mathrm{n}j}]$.

Here, we consider a ^{39}K-^{87}Rb-^{21}Ne cylindrical vapor cell at a typical condition that the temperature is $T = 190\ ^{\circ}\mathrm{C}$, filled with 50 Torr N_2, the effective pumping rate is $R_{\mathrm{op}} = 3000\ \mathrm{s}^{-1}$, the relaxation rate of electron spin is $R_{\mathrm{rel}}^{e} = 4000\ \mathrm{s}^{-1}$, the mole ratio between ^{39}K and ^{87}Rb is 0.05, the atomic density of ^{21}Ne is 3 amg, the relaxation rate for ^{21}Ne ignoring diffusion effect is mainly influenced by electric quadrupole moment of ^{21}Ne and in this simulation is $R_{\mathrm{rel}}^{n} = 0.0002\ \mathrm{s}^{-1}$ [59], the radius of the pump light is $w_0 = 0.7$ cm. For geometry, the length of the cell is $L = 1.2$ cm, the radius of the cell is $R = 0.6$ cm. For magnetic field, we employ the cell at so called compensation point $B_z = -\lambda M_{\mathrm{e}} P_{\mathrm{e}z} - \lambda M_{\mathrm{n}} P_{\mathrm{n}z}$ [60]. Under these conditions, we perform our model and obtain the relaxation rate considering the gradient of the polarization in Fermi contact interaction terms. For fundamental mode, we calculate the first 25 modes for alkali atoms and first 4 modes for noble gas to make sure the overlap integral is convergent and obtain a relaxation rate for noble gas $\frac{1}{T_{2,\mathrm{n}}^{(0)}} = 0.016\ \mathrm{s}^{-1}$ whose order of magnitude is consistent with the experimental results while we have assumed uniform longitude distribution. The corresponding EMF gradient is among $10^1 \sim 10^2\ \mathrm{nT\ cm}^{-1}$. To evaluate the order of magnitude in the $\hat{\boldsymbol{z}}$-direction, we also calculate the eigenvalues for a pair of longitude modes $u_{\mathrm{e},n}(z) = \sqrt{\frac{2}{\pi R^2 L}} \sin\frac{n\pi z}{L}$ and $u_{\mathrm{e},m}(z) = \sqrt{\frac{2}{\pi R^2 L}} \cos\frac{m\pi z}{L}$ corresponding to D-BC and N-BC, respectively, where we have assumed that the pump light is flat-topped with $f(x,y) = 1$ in equation (B5) and the diffusion mode in transverse direction is uniform. In this case, we obtain a relaxation rate $\frac{1}{T_{2,\mathrm{n}}^{(0)}} = 0.019\ \mathrm{s}^{-1}$ by calculating the first 50 modes and after convergence at around the 10th mode, the average value is taken. Thus, the gradient of the polarization is the main contribution in this condition reaching an order of $10^{-3} \sim 10^{-2}\ \mathrm{s}^{-1}$ depending on the pumping rate, transverse mode and the geometry of the cell. Numerically, we find that the EMF gradient in the $\hat{\boldsymbol{z}}$-direction is almost a constant reaching an order about $\sim 10^1\ \mathrm{nT\ cm}^{-1}$. This result could help to design gradient magnetic field coils to lower the relaxation rate of the ensemble.

4. Discussion

Besides the examples and applications above, there are also some recent research based on the consideration of analyzing or manipulating the diffusion modes in quantum optics and precision measurement, like optical

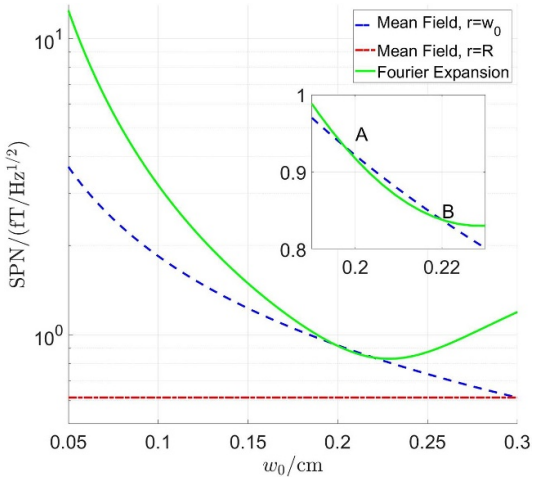

Figure 5. Calculated spin projection noise for probe light with different radii by mean field method with $V_{\rm eff}=\pi w_0^2 L$ (blue line, [43]),$V_{\rm eff}=\pi R^2 L$ (red line, [21]) and Fourier expansion method (green line, this work). A and B are the intersection points. The simulation condition is the same as figure 4.

control and coherent coupling of spin diffusive modes [61], or the analysis of the spin relaxation taking diffusion and inhomogeneous magnetic field into consideration [62], showing the agreement and validity of our methods for specific cases as shown in table 2. To emphasize the significance of our methods and the connection to quantum science and technology, in this section, we extend the discussion of our model to quantum spin projection noise. We reiterate that our model is capable of providing more rigorous relaxation rate calculations for each mode under the coupling of multi-physical fields as shown in equations (14) and (15), which will facilitate our subsequent discussion on quantum noise.

According to fluctuation-dissipation theorem, intuitively, a larger relaxation rate corresponds to a larger uncertainty and the relaxation rate has a spatial distribution due to diffusion as shown in figure 4. For a cell polarized along the $-\hat{\boldsymbol{z}}$-direction, under the approximation of Holstein-Primakoff transformation [36], we have added a random noise term in Bloch mode equations, which is essential for compensating for conservation of commutation relationship of spin operators and in turn being the quantum vacuum noise [63], to obtain the magnetic equivalent of the spin projection noise of single species alkali atomic magnetometer considering diffusion effect by

$$\delta B_x=\frac{2Q}{|\gamma_e\sum_\nu g_\nu\int_V u_{e,\nu}\mathrm{d}V|}\sqrt{\sum_\nu\frac{|g_\nu|^2}{Qn_a|\bar{P}_{ez}|T_{2,\nu}}}, \tag{24}$$

where g_ν is defined in equation (C1) while n is the atomic density. Our method contributes the value for the relaxation rate of the νth mode $\frac{1}{T_{2,\nu}}$.This result can derive the fundamental sensitivity limit $\delta B_x=\frac{Q}{\gamma_e}\sqrt{\frac{1}{n_a V_{\rm eff}T_2 t}}$ given by the mean field method [21, 43] as shown in appendix D, where $V_{\rm eff}$ is the so called active measurement volume defined by the intersection of the pump and probe laser beams [43] and t is the measuring time. We calculate the spin projection noise for probe light based on equation (24) with eigenfunctions given by equation (18) and based on mean field method as shown in in figure 5, respectively, with different radii for probe light. We make the verification for the mean field result that when the radius of the probe light is the same as the cell, i.e. $w_0=R$, the projection noise is the same since their analytical expression are the same. The so-called effective volume in this case can actually be determined by setting the radius given by the intersection point of our result and mean field lines.

In our result, we find that the measured projection noise can be adjusted by designing the shape of the cell and the mode of the probe light. From a practical perspective, this is essential since the existing technical noise such as hysteresis loss typically reach $10^0\sim10^1\mathrm{fT}/\sqrt{\mathrm{Hz}}$ @1 Hz [64, 65] so that the quantum limit could not be obtained in some ultra high sensitivity magnetometers in low frequency regime with sensitivity below technical noise. This imposes restrictions on the quantum characteristics of the cell as a macroscopic system. However, by designing the modes as discussed above, we may reach a relatively higher quantum noise, which enables us to perform quantum manipulation on such a macroscopic quantum system involving entanglement and interface, being beneficial for quantum information field [37]. From the perspective of developing, technological noise has approached levels close to quantum noise. To further enhance sensitivity,

this method can be employed to design best parameters, such as radius for probe light, to obtain a higher signal to limit noise ratio since there is a minimum for spin projection noise.

The reason for the differences in calculation of projection noise is obvious, since there must be influence resulting from spatial distribution of the fields, including gradient of light field, magnetic field, thermal field, spin field and other fields. These coupling effects actually determine the exact eigenvalues at specific position in the vapor cell, including relaxation rate and Lamor frequency, while the projection noise is related to the real part of the eigenvalues according to fluctuation-dissipation theorem. Essentially, these results are induced by the spatial quantum correlation of the spin. During the coherent time, the spin for a single atom including the projection noise, is carried by the motion of the atoms, causing the measurement taken at one place $\boldsymbol{r}$ actually including the noise exactly at $\boldsymbol{r}$ and the noise around $\boldsymbol{r}$ due to diffusion. In our result, when the radius is small (before point A), we find a larger projection noise measured by probe light since the measured atoms is less in this regime with the enhancement by mode overlap from probe light. When the radius is large (after point B), our result also becomes large even if more atoms are measured. This is because more higher order modes with larger relaxation rates are distributed around the boundary of the cell as shown in figure 4, which brings higher spin projection noise. Between point A and B, our result is approximate to the result given by mean field method. Thus, we conclude that these two methods can be highly close in some cases and our calculation is an extension to traditional mean field method rather than denying the mean field method since this improvement can degrade into mean field method if one ignores the spatial effects to the simplest form as shown in appendix D.

The study of squeezing and entanglement in macroscopic objects is an emerging and thrilling research direction in the field of quantum science due to its potential abilities in breaking through the standard measuring limits and applications in quantum technologies. This area requires effective suppression of both technical noise and quantum noise. Seminal works in thermal atomic ensemble have provided critical theoretical and experimental foundations for this field [37, 66]. However, current studies predominantly utilize simplified models ignoring the spatial distribution of various physical fields on experimental outcomes. In response to these limitations, we introduce a new method to provide a more precise calculation of quantum spin projection noise, accounting for factors previously overlooked in traditional approaches to enhance the accuracy and reliability of measurements in quantum entanglement studies. For squeezing, our result shows that for the case in 3.3, the two-mode squeezing parameter given by [37] is $\xi = 0.536$ for mean field method while our method is $\xi = 0.530$, with minor influence. However, our result has a significant influence in the entanglement time for noble gas since the relaxation rate when considering diffusion effect would raise an order due to the existence of EMF Although there are no significant differences in the case shown in figure 5, it should be noticed that in some cases when diffusion effect and multi-physics coupling are important to influence the result of projection noise, careful attention for calculation and experimental demonstration are needed to calibrate a more exact result for quantum noise, especially in some experiments like the overcoming of spin projection noise through entanglement or squeezing.

One more fresh point is the quantum noise coupling between macroscopic species. Considering a vapor cell with ^{39}K-^{3}He, if we also add random noise terms similarly as in alkali atomic ensemble above to ensure the commutation relationship conservation for both of alkali electronic spin and nuclear spin, then the two noises can be coupled by Bloch mode equations by spin exchange interaction. After a simple algebra, the coupling equations for the two species could be derived as equation (24), similar to equation (27) in [63]. The relevant calculation is complicated, so that we only show the result in the main text for brevity. The magnetic equivalent of the spin projection noise of co-magnetometer with highly polarized single species alkali atom and noble gas is

$$\delta B_x = \frac{|A|+|B|}{|A|^2+|B|^2}\sqrt{\sum_{\nu}\left[\frac{g_\nu^2}{T_{2,\nu}^a}+\sum_{\mu}g_\nu^2\left(\frac{Jc_{\mu\nu}}{T_{2,\mu}^b}\right)^2\frac{1}{T_{2,\mu}^b}\right]}. \tag{25}$$

Here, A, B and $c_{\mu,\nu}$ are coefficients related to overlap integral. In greater detail, A is related to the overlap between light and alkali atoms, while B is related to two parts: 1)the mode overlap between light and alkali atoms and 2) the mode overlap between alkali atoms and noble gas. g_ν is defined in equation (C1). $T_{2,\nu}$ is the transverse relaxation rate for the νth mode while a stands for alkali atoms and b stands for noble gas. J is the coupling constant proportional to spin-exchange rate between alkali atoms and noble gas. From equation (25), the spin projection noise is actually contributed by both alkali atoms and noble gas. The first term in the square is the same as equation (24) while the second term is coupled noise from noble gas due to the spin-exchange collisions. For a specific case, if there is no noble gas, then there must be no coupling between alkali atoms and noble gas so that $J = 0$, which implies that $B = 0$ according to appendix D. Together with the expression of A, we can see that the result is the same as equation (24), i.e. only the existence of

single species alkali atoms. In deriving equation (25), we have assumed that there is no correlation between the quantum noise of alkali atoms and noble gas. However, this would not influence the fact that the initially uncorrelated atoms would produce quantum correlation by spin exchange collisions. In fact, the noise coupling induced by spin exchange has been found in alkali atomic ensemble [67, 68]. We also evaluate the influence of coupling effects to projection noise of nuclear spin in appendix D. The result shows that the spin projection noise will be promoted comparing with no coupling case with a factor of $\eta > 1$, which is induced by the coupling from alkali atoms projection noise. Further analysis could be applied, like quantum trajectories or quantum jump. However, these discussion is beyond the contents of this paper and we only emphasize that our finding on the quantum noise coupling between alkali atoms and noble gas may lead to new chances in quantum sensing since this provides a new way for manipulating the quantum noise by spin itself rather than light-atom interactions.

The spin projection noise of two different atomic species can be coupled through spin-exchange collisions at various locations. We can see from the equation (25) that the spatial coupling indeed has an influence on the quantum noise of the spin system. The physical origin is the fact that the during spin-exchange process, both of spin and spin projection noise can be exchanged since spin projection noise is essentially a small and random spin with fluctuation. Such coupling establishes quantum correlations between alkali metals and noble gas, thereby altering the quantum spin projection noise of the noble gases. In our model, the projection noise takes similar form as noble gas in equation (D13). On the other hand, many ultra-high sensitivity measurements that extend beyond the standard model are based on nuclear spins, such as searching for the fifth force [69] and anomalous fields [25, 33]. Understanding the spin projection noise of nuclear spin is of significant importance, yet currently under-researched. Our calculation shows that in the presence of other species atoms exchanging spin with noble gas, the nuclear spin projection noise may be influenced. Thus, this method can guide corresponding research efforts and provide reference models of substantive relevance.

Another important connection to quantum science and technology of our method is related to Non-Hermitian physics. Non-Hermitian physics has been demonstrated abundant physical phenomena when the measurement is operated around EP point due to phase transition [70]. Anti-parity-time(A$\mathcal{PT}$) symmetry [71] and parity-time($\mathcal{PT}$) symmetry [72] have been achieved through atomic diffusion effects and multi-physics coupling, showing fabulous potential in sensitivity. As shown in figure 3, the signal in the two beams couple through atomic motion, with the coupling strength controllable by experimentally varying the distance between the two light sources. Our model can provide a specific analysis of coupling. This phenomenon results from the competition between the average diffusion time of the atoms from one light source to another $T_{\text{diff}} = \frac{2x_0}{\bar{v}/3}$ and the transverse relaxation time T_2. When the central distance between the light is close, i.e. $T_{\text{diff}} \ll T_2$, the coupling strength is strong and it is indistinguishable to discriminate which light polarize the atoms. When the distance becomes far, $T_{\text{diff}} \sim T_2$, the coupling strength becomes weak, but the coupling still exists. When the distance is far enough, $T_{\text{diff}} \gg T_2$, the coupling will disappear. This result could also be used for suppressing the signal crosstalk in differential gradient magnetometer in a more detail to determine the best distance between the two beams. Thus, our method actually provides a quantitative way to analyze Non-Hermitian physics in atomic ensemble induced by spatial coupling effects, which has potential in improving sensitivity and extensive understanding of quantum mechanism.

5. Conclusion

In this article, we model the spin dynamics of thermal atomic ensembles from a field perspective. The model is effective when the atomic mean free path is much shorter than the characteristic scale of the cell so that the atomic ensembles are in diffusion regime which is usually satisfied in thermal vapor cells. The Bloch mode equations of the ensembles are derived and we obtain analytical solutions for Bloch equations considering the diffusion term. This result further extends and is compatible with the existing mean field model the when the modes are purely spatially uniform. However, there are some typical spatially related problems as discussed in the introduction section that mean field model could not explain precisely. Our mode analysis approach provides a guideline of quantifying (1) the spatial multi-physic field coupling effects, such as relaxation rate induced by non-uniformity of the magnetic field gradient containing both classical magnetic field induced by the coils and EMF induced by Fermi contact interaction, (2) quantum spin projection noise considering the diffusion effect and non-uniform of the polarization, (3) spin field distribution and practical measured signal in 3 types of boundary conditions with typical shapes. Besides, the overlap integrals between the probe light and the atoms are defined, allowing for the quantitative evaluation of the contribution from each atomic mode to the overall signal. The 3D distribution of pump rate is also obtained in consistent with the field perspective during the mode analysis approach under conditions of well-collimated pump light and diffusion relaxation rate of pumped alkali atoms much smaller than other relaxation rate. The accurate calculation of relaxation rate will enable us to determine a relatively precise quantum noise according to

fluctuation-dissipation theorem. It reminds that in some experiments overcoming the quantum noise like spin squeezing and entanglement by atomic ensemble, the quantum limit should be determined carefully rather than simply calculating by mean field method.

The advantage of this approach lies in its ability to quantitatively account for coupling effects arising from the multi-physical field among environment, light and atomic ensemble, as well as within atomic ensembles. However, practical solutions sometimes require expansion to higher orders due to the mismatch between spatial mode symmetry of light (axisymmetric) and atomic diffusion (spherically symmetric in a spherical cell, for example). Furthermore, when computing overlap integrals, extensive flatten of the coefficient matrix is necessary, which significantly reduce computational efficiency, especially in cases involving a large number of mode indices in asymmetric situations. Nevertheless, once the coefficient matrix computation is completed, performing spatial operations, such as calculating polarization gradient, becomes straightforward by applying the gradient operator to the eigenfunctions. This yields results directly related to the eigenvalues, obviating the need for repetitive calculations. From this perspective, subsequent spatial analytical computations become highly convenient.

Data availability statement

All data that support the findings of this study are included within the article (and any supplementary files).

Acknowledgments

This work is supported by NSFC under Grants Nos. 62203030 and 61925301 for Distinguished Young Scholars, is also supported by the Innovation Program for Quantum Science and Technology under Grant 2021ZD0300401.

Appendix A. The derivation of the explicit form of Bloch mode equations

A.1. Single species alkali atomic ensemble

In a single-species alkali atomic vapor cell, the Bloch equation considering diffusion can be written as [53]

$$\frac{\partial \boldsymbol{P}_{\mathrm{e}}}{\partial t}=\frac{\gamma_{\mathrm{e}}}{Q}\boldsymbol{B}\times\boldsymbol{P}_{\mathrm{e}}-\frac{R_{\mathrm{op}}(\boldsymbol{r})+R_{\mathrm{rel}}}{Q}\boldsymbol{P}_{\mathrm{e}}+\frac{R_{\mathrm{op}}}{Q}\boldsymbol{s}+D_{\mathrm{e}}\nabla^{2}\boldsymbol{P}_{\mathrm{e}}, \tag{A1}$$

where $\boldsymbol{P}_{\mathrm{e}}=\boldsymbol{P}_{\mathrm{e}}(\boldsymbol{r},t)$ is the polarization at position $\boldsymbol{r}$ and time t. γ_e is gyromagnetic ratio of the bare electron. Q is the nuclear slowing down factor. $\boldsymbol{B}$ is the magnetic field. $R_{\mathrm{op}}(\boldsymbol{r})$ is the pumping rate at position $\boldsymbol{r}$. R_{rel} is the relaxation rate without diffusion and we assume that it is uniform thus independent of position as in the mean field Bloch equations. $\boldsymbol{s}$ is the average photon spin and for a right circularly polarized light propagating along z-axis we have $\boldsymbol{s}=+1\hat{\boldsymbol{z}}$. D_{e} is diffusion coefficient of the alkali atomic ensemble. The boundary is given by equation (2), where N is the average number of wall collisions a spin withstands before depolarizing [56] and $\hat{\boldsymbol{n}}$ is the outward normal unit vector at the boundary. $\bar{\lambda}=\frac{3D_{\mathrm{e}}}{2\bar{v}}$ is the mean free path of the atoms, with $\bar{v}$ being the thermal velocity. We use the eigenfunctions $\{u_n(\boldsymbol{r})\}$ of the Helmholtz equation $\nabla^2u_i(\boldsymbol{r})+k_i^2u_i(\boldsymbol{r})=0, i=1,2,3\ldots$ to expand the spin field $\boldsymbol{P}_{\mathrm{e}}=\sum_i\boldsymbol{P}_{\mathrm{e}}^{(i)}(t)u_i(\boldsymbol{r})$ so that the Bloch equation of single-species alkali atomic ensemble is given by

$$\begin{aligned}\frac{\partial}{\partial t}\sum_i\boldsymbol{P}_{\mathrm{e}}^{(i)}(t)\,u_i(\boldsymbol{r})=&\frac{\gamma_{\mathrm{e}}}{Q}\boldsymbol{B}\times\sum_i\boldsymbol{P}_{\mathrm{e}}^{(i)}(t)\,u_i(\boldsymbol{r})-\frac{R_{\mathrm{op}}(\boldsymbol{r})}{Q}\sum_i\boldsymbol{P}_{\mathrm{e}}^{(i)}(t)\,u_i(\boldsymbol{r})-\frac{R_{\mathrm{rel}}}{Q}\sum_i\boldsymbol{P}_{\mathrm{e}}^{(i)}(t)\,u_i(\boldsymbol{r})\\&+\sum_i\frac{R_{\mathrm{op}}^{(i)}u_i(\boldsymbol{r})}{Q}+D\sum_i\boldsymbol{P}_{\mathrm{e}}^{(i)}(t)\,\nabla^2u_i(\boldsymbol{r}).\end{aligned} \tag{A2}$$

Note that we do not expand $R_{\mathrm{op}}(\boldsymbol{r})$ in the nonlinear term $\frac{R_{\mathrm{op}}(\boldsymbol{r})}{Q}\boldsymbol{P}_{\mathrm{e}}(\boldsymbol{r})$ since this term could not be directly linearized when $R_{\mathrm{op}}(\boldsymbol{r})$ is non-uniform. By multiplying the equation with $u_n(\boldsymbol{r})$ and using the orthogonality of generalized Fourier functions $\int_V u_i(\boldsymbol{r})u_j(\boldsymbol{r})=\delta_{ij}$, we perform the Fourier integral to obtain the n-th Bloch mode equation,

$$\frac{\mathrm{d}\boldsymbol{P}_{\mathrm{e}}^{(n)}(t)}{\mathrm{d}t}=\gamma\boldsymbol{B}\times\boldsymbol{P}_{\mathrm{e}}^{(n)}(t)-\sum_i c_{in}\boldsymbol{P}_{\mathrm{e}}^{(i)}(t)-\frac{R_{\mathrm{rel}}}{Q}\boldsymbol{P}_{\mathrm{e}}^{(n)}(t)+\frac{R_{\mathrm{op}}^{(n)}}{Q}\boldsymbol{s}-D_{\mathrm{e}}k^{(n)2}\boldsymbol{P}_{\mathrm{e}}^{(n)}(t), \tag{A3}$$

where $c_{in}=\int_V R_{\mathrm{op}}(\boldsymbol{r})u_i(\boldsymbol{r})u_n(\boldsymbol{r})\mathrm{d}V$ is the overlap integral between light distribution and atoms diffusion mode. For simplicity, we denote $\gamma=\frac{\gamma_{\mathrm{e}}}{Q}$ as the gyromagnetic ratio of the electron considering slowing down

factor. $R_{\rm op}^{(n)}$ is the expansion coefficient of $R_{\rm op}(\boldsymbol{r})$ and represents the pumping rate for the nth atomic diffusion mode. The diffusion term automatically becomes $-D_{\rm e}k_n^2\boldsymbol{P}_{\rm e}^{(n)}(t)$ by operating Laplace operator on eigenfunctions. Thus, diffusion will bring relaxation rate $D_{\rm e}k_n^2$ for the nth mode and the relaxation rate is different for different diffusion modes. Now the problem for solving Bloch equations has been transformed into the problem of solving the expansion coefficients of the spin field, i.e. solving a matrix equation. Following the conventional Bloch equation solution method, which involves taking the steady-state solution along the pumping direction while describing the other two transverse directions using right-circular polarization component $P_{\rm e+}^{(n)}=P_{\rm ex}^{(n)}+iP_{\rm ey}^{(n)}$, we have

$$0=\frac{R_{\rm op}^{(n)}}{Q}-\sum_i c_{in}P_{\rm ez}^{(n)}-\left(\frac{R_{\rm rel}}{Q}+D_{\rm e}k_n^2\right)P_{\rm ez}^{(n)}, \tag{A4}$$

$$\frac{{\rm d}P_{\rm e+}^{(n)}}{{\rm d}t}=i\left(\omega_0P_{\rm e+}^{(n)}-\gamma B_+P_{\rm ez}^{(n)}\right)-\sum_i c_{in}P_{\rm e+}^{(n)}-\left(\frac{R_{\rm rel}}{Q}+D_{\rm e}k_n^2\right)P_{\rm e+}^{(n)} \tag{A5}$$

where $\omega_0=\frac{\gamma_{\rm e}}{Q}B_z$ is the Lamor precession frequency and $B_+=B_x+iB_y$ is the complex magnetic field in the transverse plane. The dynamic equations can be simplified to equations (3) and (4) by defining

$$\mathcal{P}_{\rm ez}=\begin{pmatrix}P_{\rm ez}^{(1)}\\P_{\rm ez}^{(2)}\\P_{\rm ez}^{(3)}\\\vdots\\P_{\rm ez}^{(n)}\\\vdots\end{pmatrix},\mathcal{P}_{\rm e+}=\begin{pmatrix}P_{\rm e+}^{(1)}\\P_{\rm e+}^{(2)}\\P_{\rm e+}^{(3)}\\\vdots\\P_{\rm e+}^{(n)}\\\vdots\end{pmatrix},\mathcal{R}=\frac{1}{Q}\begin{pmatrix}R_{\rm op}^{(1)}\\R_{\rm op}^{(2)}\\R_{\rm op}^{(3)}\\\vdots\\R_{\rm op}^{(n)}\\\vdots\end{pmatrix},\mathcal{C}=\frac{1}{Q}\begin{pmatrix}c_{11}&c_{21}&c_{31}&\dots&c_{n1}&\cdots\\c_{12}&c_{22}&c_{32}&\dots&c_{n2}&\cdots\\c_{13}&c_{23}&c_{33}&\dots&c_{n3}&\cdots\\\vdots&\vdots&\vdots&\ddots&\vdots&\dots\\c_{1n}&c_{2n}&c_{3n}&\dots&c_{nn}&\cdots\\\vdots&\vdots&\vdots&\ddots&\vdots&\dots\end{pmatrix},$$

$$\mathcal{K}=D_{\rm e}\begin{pmatrix}k_1^2&0&\cdots&0&\cdots\\0&k_2^2&\cdots&0&\cdots\\\vdots&\vdots&\ddots&\vdots&\cdots\\0&0&\cdots&k_n^2&\cdots\\\vdots&\vdots&\ddots&\vdots&\cdots\end{pmatrix}+\frac{R_{\rm rel}}{Q}\mathcal{I},\mathcal{A}=\mathcal{C}+\mathcal{K},\Omega=\frac{\gamma_e}{Q}B_z\mathcal{I},\Omega_+=\frac{\gamma_e}{Q}B_+\mathcal{I}. \tag{A6}$$

where $\mathcal{I}$ is unit matrix.

A.2. Hybrid alkali atomic ensemble

In the case of a hybrid alkali atomic vapor cell containing elements such as ^{39}K and ^{87}Rb, we consider the case where the pump light frequency matches the D1 line of $\mathcal{D}_1$ line of ^{39}K and propagates along the $\hat{\boldsymbol{z}}$-direction. In this case, ^{39}K is pumped by pump light and ^{87}Rb is pumped by the fast exchange collisions with polarized ^{39}K to achieve a uniform polarization. The dynamics of the two-species atoms can be described by the following Bloch equations [54]

$$\frac{\partial}{\partial t}\boldsymbol{P}^d=\frac{\gamma_e}{Q^d}\boldsymbol{B}\times\boldsymbol{P}^d+\frac{R_{\rm ex}^{\rm dr}}{Q^d}\left(\boldsymbol{P}^r-\boldsymbol{P}^d\right)-\frac{R_{\rm rel}^d}{Q^d}\boldsymbol{P}^d-\frac{R_{\rm op}(\boldsymbol{r})}{Q^d}\boldsymbol{P}^d+\frac{R_{\rm op}}{Q^d}\boldsymbol{s}+D^d\nabla^2\boldsymbol{P}^d, \tag{A7}$$

$$\frac{\partial}{\partial t}\boldsymbol{P}^r=\frac{\gamma_e}{Q^r}\boldsymbol{B}\times\boldsymbol{P}^r+\frac{R_{\rm ex}^{\rm rd}}{Q^r}\left(\boldsymbol{P}^d-\boldsymbol{P}^r\right)-\frac{R_{\rm rel}^r}{Q^r}\boldsymbol{P}^r+D^r\nabla^2\boldsymbol{P}^r. \tag{A8}$$

Here, the index d denotes 'donor', implying that this type of atomic ensemble, such as ^{39}K, donates its spin to another type, such as ^{87}Rb, which is the spin receiver denoted by r, through rapid spin-exchange collisions. $R_{\rm ex}^{\rm dr}=n_r\left\langle\sigma_{\rm se}^{\rm dr}\bar{v}_{\rm dr}\right\rangle$ is the spin exchange rate of the donor atoms and $R_{\rm ex}^{\rm rd}=n_d\left\langle\sigma_{\rm se}^{\rm rd}\bar{v}_{\rm rd}\right\rangle$ is the spin exchange rate of the receiver atoms, where $\sigma_{\rm se}^{\rm dr}$ is the spin exchange collisional cross-section and $\bar{v}_{\rm dr}$ is the relative thermal velocity between donor atoms and receiver atoms. Similarly, by expansion and denoting

$$\mathcal{J}^{\mathrm{dr}}=\begin{pmatrix} j_{11} & j_{12} & \cdots & j_{1m} & \cdots \\ j_{21} & j_{22} & \cdots & j_{2m} & \cdots \\ \vdots & \vdots & \ddots & \vdots & \cdots \\ j_{n1} & j_{n2} & \cdots & j_{nm} & \cdots \\ \vdots & \vdots & \ddots & \vdots & \cdots \end{pmatrix}, \mathcal{J}^{\mathrm{rd}}=\left(\mathcal{J}^{\mathrm{dr}}\right)^{T}, \tag{A9}$$

$$\mathcal{P}_{z,nm\times 1}=\begin{pmatrix} \mathcal{P}_z^d \\ \mathcal{P}_z^r \end{pmatrix}, \mathcal{P}_{+}=\begin{pmatrix} \mathcal{P}_+^d \\ \mathcal{P}_+^r \end{pmatrix}, \tag{A10}$$

$$\mathcal{R}^{d-r}=\frac{1}{Q}\begin{pmatrix} R_{\mathrm{op}}^{(1)} & R_{\mathrm{op}}^{(2)} & \cdots & R_{\mathrm{op}}^{(n)} & \mathbf{0}_{1\times m} \end{pmatrix}^{T}, \tag{A11}$$

$$\mathcal{C}^{d-r}=\begin{pmatrix} \mathcal{C}_{n\times n} & \mathbf{0}_{n\times m} \\ \mathbf{0}_{m\times n} & \mathbf{0}_{m\times m} \end{pmatrix}, \tag{A12}$$

$$\mathcal{K}^{d-r}=\begin{pmatrix} \mathcal{K}_{n\times n}^{r} & \mathbf{0}_{n\times m} \\ \mathbf{0}_{m\times n} & \mathcal{K}_{m\times m}^{d} \end{pmatrix}, \tag{A13}$$

$$\mathcal{J}^{d-r}=\begin{pmatrix} \mathbf{0}_{n\times n} & \frac{R_{\mathrm{ex}}^{\mathrm{dr}}}{Q^d}\mathcal{J}_{n\times m}^{\mathrm{dr}} \\ \frac{R_{\mathrm{ex}}^{\mathrm{rd}}}{Q^r}\mathcal{J}_{m\times n}^{\mathrm{rd}} & \mathbf{0}_{m\times m} \end{pmatrix}, \tag{A14}$$

$$\mathcal{A}^{d-r}=\mathcal{C}^{d-r}+\mathcal{K}^{d-r}-\mathcal{J}^{d-r} \tag{A15}$$

$$\Omega^{d-r}=\begin{pmatrix} \frac{\gamma_e}{Q^d}B_z\mathcal{I}_{n\times n} & \mathbf{0}_{n\times m} \\ \mathbf{0}_{m\times n} & \frac{\gamma_e}{Q^r}B_z\mathcal{I}_{m\times m} \end{pmatrix}, \tag{A16}$$

$$\Omega_{+}^{d-r}=\begin{pmatrix} \frac{\gamma_e}{Q^d}B_+\mathcal{I}_{n\times n} & \mathbf{0}_{n\times m} \\ \mathbf{0}_{m\times n} & \frac{\gamma_e}{Q^r}B_+\mathcal{I}_{m\times m} \end{pmatrix}, \tag{A17}$$

where definitions of the individual block matrices such as $\mathcal{K}^r$ and $\mathcal{K}^d$ are consistent with those defined in equation (A6) while the matrix elements are defined by

$$j_{kn}=\int u_r^{(k)}u_d^{(n)}dV, \tag{A18}$$

$$c_{in}=\int R_{\mathrm{op}}(\boldsymbol{r})\,u_d^{(i)}u_d^{(n)}\mathrm{d}V, \tag{A19}$$

$$R_{\mathrm{op}}^{(n)}=\int R_{\mathrm{op}}(\boldsymbol{r})\,u_d^{(n)}\mathrm{d}V. \tag{A20}$$

Consequently, the mode equations can be simplified to equations (3) and (4).

A.3. Alkali-nobal gas atomic ensemble

For a hybrid alkali-noble gas atomic vapor cell, the Bloch equations for describing the ensembles are as follows [55]:

$$\frac{\partial \boldsymbol{P}^e}{\partial t}=\frac{\gamma_e}{Q}\left(\boldsymbol{B}+\lambda M_n\boldsymbol{P}^n\right)\times\boldsymbol{P}^e+\frac{1}{Q}\left(R_{\mathrm{op}}\boldsymbol{s}_{\mathrm{p}}+R_{\mathrm{se}}^{\mathrm{en}}\boldsymbol{P}^n-R_{\mathrm{tot}}^{e}\boldsymbol{P}^e\right)+D^e\nabla^2\boldsymbol{P}^e, \tag{A21}$$

$$\frac{\partial \boldsymbol{P}^n}{\partial t}=\gamma_n\left(\boldsymbol{B}+\lambda M_e\boldsymbol{P}^e\right)\times\boldsymbol{P}^n+R_{\mathrm{se}}^{\mathrm{ne}}\boldsymbol{P}^e-R_{\mathrm{tot}}^{n}\boldsymbol{P}^n+D^n\nabla^2\boldsymbol{P}^n, \tag{A22}$$

where $\boldsymbol{P}^e$ is the effective spin field of the electron and $\boldsymbol{P}^n$ is the spin field of the noble gas. γ_n is the nuclear gyromagnetic ratio of noble gas. $\lambda M_n\boldsymbol{P}^n$ is the EMF of noble gas due to Fermi-contact interaction between alkali and noble gas and $\lambda M_e\boldsymbol{P}^e$ of electron. Additionally, we have disregarded the anomalous force and angular velocity input terms, under the ideal assumption that there is no pumping effect in purely linearly polarized probe light. Here, R_{tot}^r and R_{op} could be regarded as a constant since the strong coupling between two hybrid alkali species enables the spin field to be more uniform and thus effective pumping rate is also uniform due to the diffusion. $R_{\mathrm{se}}^{\mathrm{en}}$ is the spin exchange rate experienced by electron and $R_{\mathrm{se}}^{\mathrm{en}}$ is the spin exchange rate experienced by noble gas.

By similar expansion and denoting

$$\mathcal{K}^e = D^e \mathrm{diag}\left\{k_1^{(e)2}, k_2^{(e)2}, \ldots, k_n^{(e)2}\right\} + \frac{R_{\mathrm{tot}}^e}{Q}\mathcal{I}_{n\times n},$$
$$\mathcal{K}^n = D^n \mathrm{diag}\left\{k_1^{(n)2}, k_2^{(n)2}, \ldots, k_m^{(n)2}\right\} + R_{\mathrm{tot}}^n \mathcal{I}_{m\times m},$$
$$\mathcal{J}^{e-n} = \begin{pmatrix} \mathbf{0} & \frac{R_{\mathrm{se}}^{\mathrm{en}}}{Q}\mathcal{J}_{n\times m}^{\mathrm{en}} \\ R_{\mathrm{se}}^{\mathrm{ne}}\mathcal{J}_{m\times n}^{\mathrm{ne}} & \mathbf{0} \end{pmatrix}, \mathcal{K}^{e-n} = \begin{pmatrix} \mathcal{K}^e & \mathbf{0} \\ \mathbf{0} & \mathcal{K}^n \end{pmatrix}, \mathcal{A}^{e-n} = \mathcal{K}^{e-n} - \mathcal{J}^{e-n},$$
$$\mathcal{H}_{(n+m)\times(n+m)}^{e-n} = \begin{pmatrix} \frac{\gamma_e}{Q}\lambda M_n \mathcal{H}^e\left(\mathcal{P}_{nz}\otimes \mathbf{1}_{n\times n}\right) & -\frac{\gamma_e}{Q}\lambda M_n \mathcal{H}^e\left(\mathcal{P}_{ez}\otimes \mathbf{1}_{m\times m}\right) \\ -\gamma_n \lambda M_e \mathcal{H}^n\left(\mathcal{P}_{nz}\otimes \mathbf{1}_{n\times n}\right) & \gamma_n \lambda M_e \mathcal{H}^n\left(\mathcal{P}_{ez}\otimes \mathbf{1}_{m\times m}\right) \end{pmatrix},$$
$$\mathcal{H}^e = \mathcal{H}_{n\times nm}^e = \begin{pmatrix} \mathcal{H}_{(1)}^e \\ \mathcal{H}_{(2)}^e \\ \vdots \\ \mathcal{H}_{(n)}^e \end{pmatrix}, \mathcal{H}^n = \mathcal{H}_{m\times nm}^n = \begin{pmatrix} \mathcal{H}_{(1)}^n \\ \mathcal{H}_{(2)}^n \\ \vdots \\ \mathcal{H}_{(m)}^n \end{pmatrix},$$
$$\mathcal{H}_{(i)}^e = \left(h_{i11}^{(e)} \quad h_{i12}^{(e)} \quad \cdots \quad h_{i1n}^{(e)} \,\middle|\, h_{i21}^{(e)} \quad h_{i22}^{(e)} \quad \cdots \quad h_{i2n}^{(e)} \,\middle|\, \cdots \,\middle|\, h_{im1}^{(e)} \quad h_{im2}^{(e)} \quad \cdots \quad h_{imn}^{(e)} \right)_{1\times nm}, \quad i = 1,2,\ldots,n$$
$$\mathcal{H}_{(j)}^n = \left(h_{j11}^{(n)} \quad h_{j12}^{(n)} \quad \cdots \quad h_{j1n}^{(n)} \,\middle|\, h_{j21}^{(n)} \quad h_{j22}^{(n)} \quad \cdots \quad h_{j2n}^{(n)} \,\middle|\, \cdots \,\middle|\, h_{jm1}^{(n)} \quad h_{jm2}^{(n)} \quad \cdots \quad h_{jmn}^{(n)} \right)_{1\times nm}, \quad j = 1,2,\ldots,m$$
$$h_{ijk}^{(e)} = \int_V u_e^{(i)} u_n^{(j)} u_e^{(k)} \mathrm{d}V, h_{ijk}^{(n)} = \int_V u_n^{(i)} u_e^{(j)} u_n^{(k)} \mathrm{d}V,$$
$$\Omega^{e-n} = \begin{pmatrix} \frac{\gamma_e}{Q}B_z\mathcal{I} & \mathbf{0} \\ \mathbf{0} & \gamma_n B_z \mathcal{I} \end{pmatrix} + \mathcal{H}^{e-n}, \Omega_+^{e-n} = \begin{pmatrix} \frac{\gamma_e}{Q}B_+\mathcal{I} & \mathbf{0} \\ \mathbf{0} & \gamma_n B_+ \mathcal{I} \end{pmatrix}, \mathcal{P}_+ = \begin{pmatrix} \mathcal{P}_{e,+} \\ \mathcal{P}_{n,+} \end{pmatrix}. \tag{A23}$$

Again, the mode equations for alkali-noble gas atomic ensemble are simplified to equations (3) and (4).

Appendix B. The derivation of pumping rate in 3D

The definition of R_{op} is

$$R_{\mathrm{op}} = \frac{P\sigma}{h\nu}, \tag{B1}$$

where P is the power density of the pump light whose unit is W m^{-2}. σ is the absorption cross-section, h is Plank constant. ν is the central frequency of the pump light and the term $\Phi(\nu) = \frac{P}{h\nu}$ is refered to the total flux of photons of frequency ν incident on the atom in units of number of photons per area per time [53]. P has been regarded as a constant or as a function only in $\hat{\boldsymbol{z}}$-direction, i.e. $P = P(z)$, in the mean field method. Nevertheless, except for flat-topped light beams, almost all the light has a transverse mode distribution, for example, Gaussian mode $P_G = P_0 e^{-\frac{2\rho^2}{w_0^2}}$, where w_0 is the beam waist radius. That means, in fact, the power of the pump light is a 3D function $P = P(x,y,z)$.

We assume that the absorption of the light will not change the transverse distribution of the light for a well-collimated pump light whose divergence is negligible within the vapor cell. That means we can perform a separation of variables on the pump light power density $P(x,y,z) = I(z)\frac{f(x,y)}{A}$, where $I(z)$ is the effective power of the pump light at z-plane, $f(x,y)$ is the normalized transverse distribution of the light and A is the normalization coefficient with an area dimension m^2 whose physical significance is the effective cross-section of the light. In this way, the reduction of the pumping rate R_{op} along $\hat{\boldsymbol{z}}$-direction is given by

$$\frac{\partial}{\partial z}R_{\mathrm{op}}(x,y,z) = -n\sigma R_{\mathrm{op}}(x,y,z)\left(1 - \boldsymbol{s}\cdot\hat{\boldsymbol{z}}P_{\mathrm{ez}}\right), \tag{B2}$$

where $\boldsymbol{s}$ is the average photon spin for describing the polarization of the pump light [53]. $P_{\mathrm{ez}} \approx \frac{R_{\mathrm{op}}(\boldsymbol{r})}{R_{\mathrm{op}}(\boldsymbol{r})+R_{\mathrm{rel}}}$ is the steady solution for z-component polarization without considering diffusion effect of the atoms since for pumped alkali atomic ensemble the relaxation rate due to diffusion effect is negligible ($10^0 \sim 10^1$ s^{-1}) compared to other relaxation processes such as spin destruction collision (typically $10^2 \sim 10^3$ s^{-1}) in most cases [73]. Based on the fact above, we have assumed that the relaxation rate induced by diffusion is negligible compared to the sum of other relaxation rate R_{rel}. There are two typical boundary conditions for equation (B2). One scenario that could obtain strict analytical solution is when the incident pump light reaches the surface of the cell as a flat plane like a cube-shape cell

$$R_{\mathrm{op}}(x,y,0) = \frac{I(0)f(x,y)\sigma}{Ah\nu}, \tag{B3}$$

where $I(0)$ is the power of the pump light at $z=0$ plane. The other one is when the chamber surface Ω is curved like a spherical cell or the curve surface of a cylindrical cell

$$R_{\mathrm{op}}(x,y,z)=\left.\frac{I(z)f(x,y)\sigma}{Ah\nu}\right|_{(x,y,z)\in\Omega}. \tag{B4}$$

For the flat plane boundary case, the equation can be solved with the help of Lambert W function which is the inverse function of $f(W)=We^{W}$ and is also referred to as the product log

$$R_{\mathrm{op}}(x,y,z)=R_{\mathrm{rel}}W\left(A(x,y)\,e^{-n\sigma(\nu_0)z+A(x,y)}\right), \tag{B5}$$

where

$$A(x,y)=\frac{R_{\mathrm{op}}(x,y,0)}{R_{\mathrm{rel}}}. \tag{B6}$$

For cylindrical vapor cell with pump light propagating along the axial direction of cylinder cell, one just need to employ the transformation of coordinates $x=\rho\cos\phi$ and $y=\rho\sin\phi$ to equation (B5) to obtain $R_{\mathrm{op}}(\rho,\phi,z)$ in cylindrical coordinate. For symmetry case, equation (11) is otained.

For the curved surface boundary case in spherical vapor, we obtain

$$R_{\mathrm{op}}(r,\theta,\phi)=R_{\mathrm{rel}}W\left(A(r,\theta,\phi)\,e^{-n\sigma(r\cos\theta-R)+A(r,\theta,\phi)}\right), \tag{B7}$$

where

$$A(r,\theta,\phi)=\frac{R_{\mathrm{op},0}f(r,\theta,\phi)}{R_{\mathrm{rel}}}. \tag{B8}$$

$f(r,\theta,\phi)$ is the normalized transverse distribution function of light. Specially, for Gaussian beam, we have $f_G(r,\theta)=\sqrt{4/\pi Lw_0^2}e^{-2\frac{r^2\sin^2\theta}{w_0^2}}$. Note that R_{op0} is the initial pumping rate at $r=R,\theta=\pi$ in the spherical vapor cell since we have assumed that the pump light is propagating along z-axis and the center of the cell is at $r=0$. The general solution of the equation equation (B2) is given by

$$R_{\mathrm{op}}(x,y,z)=R_{\mathrm{rel}}W\left(\frac{C(x,y)}{R_{\mathrm{rel}}}e^{-n\sigma z}\right) \tag{B9}$$

where $C(x,y)$ is the undetermined function which should be given by boundary condition equation (B4). For a spherical vapor cell, one might naturally but incorrectly consider using a projection to map the initial position's extraction rate distribution at $z=-R$ to the sphere's surface. This is wrong since the beam propagates in the $\hat{\boldsymbol{z}}$-direction, its total energy is absorbed and this absorption is related to the internal atomic states, i.e. it is related to the general solution of the equation (B9). Therefore, this creates a paradox, meaning that one must know the light attenuation to determine the light's boundaries, while on the other hand, one must know the light's boundary condition to determine the light attenuation.

We adopt an approximation in which the absorption does not alter the pump light's transverse distribution. This approximation is valid when the pump light is well-collimated. Thus, according to equation (B9) at $z=-R$

$$R_{\mathrm{op}}(x,y,-R)=R_{\mathrm{rel}}W\left(\frac{C(x,y)}{R_{\mathrm{rel}}}e^{n\sigma R}\right). \tag{B10}$$

With the properties of the Lambert W function, we obtain

$$C(x,y)=R_{\mathrm{op},0}e^{n\sigma R+\frac{R_{\mathrm{op},0}}{R_{\mathrm{rel}}}}. \tag{B11}$$

Substitute equation (B11) into equation (B9) and we can obtain equation (B7) by transformation of coordinate $x=r\sin\theta\cos\phi$, $y=r\sin\theta\sin\phi$, and $z=r\cos\theta$ with the denoting of equation (B8).

Appendix C. The overlap integral of the light and atomic ensemble.

We assume the attenuation of the probe beam within the cell is negligible due to large detuning from the absorption frequency so that is uniform along propagation direction and the mode of the probe light is $I_{\mathrm{p}}(\boldsymbol{r}) = I_0 f(\boldsymbol{r})$ where I_0 is mode normalization coefficient and $f(\boldsymbol{r})$ is the transverse distribution, for example, Gaussian distribution $f_G(\boldsymbol{r}) = e^{-\frac{2\rho^2}{w_0^2}}$. Here, the mode of the probe light is normalized by $\int_V I_{\mathrm{p}}^2(\boldsymbol{r})\mathrm{d}V = 1$ so that $I_0^{-2} = \int f^2(\boldsymbol{r})\mathrm{d}V$. Then we employ the eigenfunction of atoms to expand the probe light mode by $I_{\mathrm{p}}(\boldsymbol{r}) = \sum_i I_i u_i(\boldsymbol{r})$. In this way, the overlap integral between probe light mode and the ith atomic diffusion mode is given by

$$g_n = \int_V I_{\mathrm{p}}(\boldsymbol{r})\, u_n(\boldsymbol{r})\, \mathrm{d}V = \sum_i I_i h_{in}, \tag{C1}$$

where h_{in} is defined by $h_{in} = \int_V u_i(\boldsymbol{r}) u_n(\boldsymbol{r})\mathrm{d}V$. We denote the matrix composed by h_{ij} as $\mathcal{H}$. The overlap integral describes the contribution weight of each order of diffusion mode of alkali metal atoms to the final signal. Therefore, taking the overlap integral into consideration, the $P_{\mathrm{s},+}$ measured at the position $\boldsymbol{r}$ and time t by the probe light is

$$P_{\mathrm{s},+m}(\boldsymbol{r}, t) = \left(\mathcal{I}_{\mathrm{p}} \mathcal{H} \mathcal{P}_{\mathrm{s},+}\right)^T \mathcal{U}_{\mathrm{s}}(\boldsymbol{r}), \tag{C2}$$

where

$$\begin{aligned} \mathcal{I}_{\mathrm{p}} &= \mathrm{diag}\{I_1, I_2, \ldots, I_n\}, \\ \mathcal{H} &= \begin{pmatrix} h_{11} & h_{12} & \cdots & h_{1n} \\ h_{21} & h_{22} & \cdots & h_{2n} \\ \vdots & \vdots & \ddots & \vdots \\ h_{n1} & h_{n2} & \cdots & h_{nn} \end{pmatrix}. \end{aligned} \tag{C3}$$

The final measured signal I_m is proportional to the average value of $P_{\mathrm{s},+m}$ due to Faraday rotation in a continuous measurement with integration time τ in the detection devices such as photon detector (PD)

$$I_m \propto \bar{P}_{\mathrm{s},+m} = \frac{1}{\tau}\int_0^\tau \left[\frac{1}{V}\int_V P_{\mathrm{s},+m}(\boldsymbol{r}, t)\, \mathrm{d}V\right] \mathrm{d}t. \tag{C4}$$

Appendix D. The derivation of projection noise for alkali atomic ensemble considering diffusion

To derive the projection noise for an alkali atomic ensemble, we assume uniform polarization in the $\hat{\boldsymbol{z}}$-direction which could be realized by two pump light propagating along the opposite direction and the atoms are pumped along the $-\hat{\boldsymbol{z}}$-direction, so that we could employ Holstein-Primakoff transformation on the density of collective transverse components [36, 63], i.e. $a = \sqrt{Qn_a/|\bar{P}_{\mathrm{ez}}|}P_{\mathrm{e}+}/2$, where n_a is the atomic number density of alkali atoms. We have regard P_{ez} as a constant $|\bar{P}_{\mathrm{ez}}|$ which is the average value of polarization of alkali atomic ensemble and regarded $P_{\mathrm{e}+}^{(\nu)} = 2(S_x - iS_y)$ as an operator. In this assumption, the equation for the νth mode of a now becomes

$$\frac{\mathrm{d}a_\nu}{\mathrm{d}t} = \left(i\omega_0 - \frac{1}{T_{2,\nu}}\right) a_\nu - i r_\nu B_- + f_\nu, \tag{D1}$$

where the coefficient $r_\nu = \frac{\gamma_{\mathrm{e}}}{Q}\frac{\sqrt{Qn_a|\bar{P}_{\mathrm{e},z}|}}{2}\int_V u_{\mathrm{e},\nu}(\boldsymbol{r})\mathrm{d}V$ and $\frac{1}{T_{2,\nu}} = \left(\frac{R_{\mathrm{rel}}}{Q} + D_{\mathrm{e}}k_\nu^2\right)$ is the relaxation rate for the νth mode of a. The term f_ν reprensents random noise for compensating commutation relationship and the spin noise operator holds $\left\langle f_\nu(t) f_\nu^\dagger(t')\right\rangle = \frac{2}{T_{2,\nu}}\delta(t - t')$ and $\left\langle f_\nu^\dagger(t) f_\nu(t')\right\rangle = 0$ according to [36]. Taking overlap integral into consideration, we solve the equation above

$$B_- = \frac{\sum_\nu g_\nu \left[i(\omega - \omega_0) + \frac{1}{T_{2,\nu}}\right] a_\nu}{i\sum_\nu g_\nu r_\nu} + \frac{\sum_\nu g_\nu f_\nu}{\sum_\nu g_\nu r_\nu}. \tag{D2}$$

The first term stands for the magnetic equivalent of measured signal while the second term is the magnetic equivalent of spin projection noise. So that by substituting the noise moment into the signal, the magnetic equivalent of the spin projection noise is

$$\delta B_x = \frac{2Q}{|\gamma_e \sum_\nu g_\nu \int_V u_{e,\nu} \mathrm{d}V|} \sqrt{\sum_\nu \frac{|g_\nu|^2}{Q n_a |\bar{P}_{ez}| T_{2,\nu}}} \tag{D3}$$

as shown in equation (24) where we have used $\delta B_- = \sqrt{2}\delta B_x$. Specially, for $I = 3/2$ alkali atomic SERF magnetometer operating at the most sensitive parameter for polarization $|\bar{P}_{ez}| = 0.5$ with uniform mode of overlap integral $g_\nu = 1$, and uniform mode of diffusion $u_{e,\nu} = 1/\sqrt{V}$ and $T_{2,\nu} = T_2$, taking the bandwidth for measuring $\mathrm{BW} = 1/2t$ with t being the measuring time into consideration [43], setting $\gamma = \frac{\gamma_e}{Q}$, we obtain

$$\delta B_{x,\mathrm{u}} = \frac{1}{\gamma}\sqrt{\frac{\mathrm{BW}}{0.5 n_a V T_2}\frac{4}{Q}} \approx \frac{1}{\gamma}\sqrt{\frac{2\mathrm{BW}}{n_a V T_2}} = \frac{1}{\gamma}\sqrt{\frac{1}{n_a V T_2 t}}, \tag{D4}$$

which is the same as the spin projection noise given by mean field method [21, 43]. We have used the same approximation condition as mean field method by $Q \approx 4$ for $I = 3/2$ alkali atoms in deriving equation (D4).

The mode coupling equations for alkali atoms and noble gas are given by equation (27) of [63]

$$\begin{aligned} \frac{\mathrm{d}a_\nu}{\mathrm{d}t} &= \left(i\omega_a - \frac{1}{T^a_{2,\nu}}\right) a_\nu - \sum_\mu i J c_{\mu\nu} b_\mu + i r_\nu B_- + f_{a,\nu}, \\ \frac{\mathrm{d}b_\mu}{\mathrm{d}t} &= \left(i\omega_b - \frac{1}{T^b_{2,\mu}}\right) b_\nu - \sum_\lambda i J c^*_{\mu\lambda} a_\lambda + i\frac{r_\mu}{\phi} B_- + f_{b,\mu}. \end{aligned} \tag{D5}$$

Here, a stands for alkali atoms and b stands for noble gas. $\omega_{a/b}$ is the Lamor frequency for a/b. $T^a_{2,\nu}$ is the transverse relaxation rate for the νth mode of alkali atoms and in a similar way for $T^b_{2,\mu}$. J is the coherent spin-exchange rate and ϕ is the phase induced by spin-exchange, both of which are defined in [63].
$r_\nu = \frac{\gamma_e}{Q}\frac{\sqrt{Q n_a |\bar{P}_{e,z}|}}{2}\int_V u_{e,\nu}(\boldsymbol{r})\mathrm{d}V$ stands for the spin response to transverse magnetic field B_- and
$r_\mu = \frac{\gamma_e}{Q}\frac{\sqrt{Q n_a |\bar{P}_{e,z}|}}{2}\int_V u_{n,\nu}(\boldsymbol{r})\mathrm{d}V$. $c_{\mu\nu} = \int_V u_{n,\mu} u_{e,\nu}\mathrm{d}V$ is the overlap integral between alkali atoms and noble gas. The solution for the coupled mode equations is

$$\begin{aligned} B_- = &\frac{\sum_\nu g_\nu \left(i(\omega-\omega_a) + 1/T^a_{2,\nu}\right) a_\nu(t)}{\sum_\nu g_\nu \left(i r_\nu + \sum_\mu J\left(\frac{r_\mu}{\phi}\frac{c_{\mu\nu}}{i(\omega-\omega_b)+T^b_{2,\mu}}\right)\right)} + \frac{\sum_\nu \sum_\mu iJ\left(\frac{-\sum_\lambda iJ a_\lambda(t) c^*_{\mu\lambda} g_\nu c_{\mu\nu}}{i(\omega-\omega_b)+T^b_{2,\mu}}\right)}{\sum_\nu g_\nu \left(i r_\nu + \sum_\mu J\left(\frac{r_\mu}{\phi}\frac{c_{\mu\nu}}{i(\omega-\omega_b)+T^b_{2,\mu}}\right)\right)} \\ &- \frac{\sum_\nu g_\nu f_{a,\nu}(t)}{\sum_\nu g_\nu \left(i r_\nu + \sum_\mu J\left(\frac{r_\mu}{\phi}\frac{c_{\mu\nu}}{i(\omega-\omega_b)+T^b_{2,\mu}}\right)\right)} + \frac{\sum_\nu \sum_\mu iJ\left(\frac{f_{b,\mu}(t) g_\nu c_{\mu\nu}}{i(\omega-\omega_b)+T^b_{2,\mu}}\right)}{\sum_\nu g_\nu \left(i r_\nu + \sum_\mu J\left(\frac{r_\mu}{\phi}\frac{c_{\mu\nu}}{i(\omega-\omega_b)+T^b_{\mu}}\right)\right)}. \end{aligned} \tag{D6}$$

The first line is the alkali atomic response to magnetic field. The second line is the noble gas response to magnetic field coupling to alkali atoms. The third line is the magnetic equivalent of spin projection noise for alkali atoms and The last line is the magnetic equivalent of spin projection noise for noble gas coupling to alkali atoms. Here, we see clearly that the measured signal is composed by first two lines of magnetic responses and last two lines of noises. By setting $J = 0$, i.e. if the case is that there is no coupling between alkali atoms and noble gas such as applying a large magnetic field in z direction, then the real part of the result can be simplified to equation (D2), which is obvious in physics and we show it mathematically to make a verification. Similar to equation (D3), we can derive the the magnetic magnetic equivalent of spin projection noise for alkali atoms in the presence of the coupling from noble gas by transforming the rotation coordinate system into the Lamor frequency of noble gas ω_b so that the term $\omega - \omega_b$ could be eliminated. By doing so, we obtain

$$\delta B_x = \frac{|A| + |B|}{|A|^2 + |B|^2}\sqrt{\sum_\nu \left[\frac{g^2_\nu}{T^a_{2,\nu}} + \sum_\mu g^2_\nu \left(\frac{J c_{\mu\nu}}{T^b_{2,\mu}}\right)^2 \frac{1}{T^b_{2,\mu}}\right]} \tag{D7}$$

where

$$A = \sum_{\nu} g_{\nu} r_{\nu}, \tag{D8}$$

$$B = \sum_{\nu} g_{\nu} \sum_{\mu} J\left(\frac{r_{\mu} c_{\mu\nu} T_{2,\mu}^{b}}{\phi}\right), \tag{D9}$$

$$c_{\mu\nu} = \int_{V} u_{b,\mu}(\boldsymbol{r})\, u_{e,\nu}(\boldsymbol{r})\, \mathrm{d}^{3}\boldsymbol{r}, \tag{D10}$$

$$r = \frac{\gamma_{\mathrm{e}}}{Q} \frac{\sqrt{Q n_{a} |\bar{P}_{\mathrm{e},z}|}}{2}, \tag{D11}$$

$$r_{\nu} = r \int_{V} u_{\nu}^{a}(\boldsymbol{r})\, \mathrm{d}^{3}\boldsymbol{r}, r_{\mu} = r \int_{V} u_{\mu}^{b}(\boldsymbol{r})\, \mathrm{d}^{3}\boldsymbol{r}. \tag{D12}$$

Similarly, we obtain the magnetic equivalent of nuclear spin projection noise without overlap integral for the m-th mode

$$\delta B_{x,m} = \frac{|C_m| + |D_m|}{|C_m|^2 + |D_m|^2} \sqrt{\frac{1}{T_{2,m}^{b}} + \sum_{k} J^2 \left(\frac{c_{mk}}{T_{2,k}^{a}}\right)^2 \frac{1}{T_{2,k}^{a}}} \tag{D13}$$

where

$$C_m = \frac{r_m}{\phi}, \tag{D14}$$

$$D_m = J \sum_{k} r_k c_{mk} T_{2,k}^{a} \tag{D15}$$

$$c_{mk} = \int_{V} u_{e,m}(\boldsymbol{r})\, u_{b,k}(\boldsymbol{r})\, \mathrm{d}^{3}\boldsymbol{r}, \tag{D16}$$

$$r_m = r \int_{V} u_{m}^{b}(\boldsymbol{r})\, \mathrm{d}^{3}\boldsymbol{r}, \tag{D17}$$

$$\phi = \frac{\gamma_{\mathrm{e}}}{Q\gamma_{\mathrm{n}}} \sqrt{\frac{Q n_{a} |\bar{P}_{\mathrm{e,z}}|}{n_{b} |\bar{P}_{\mathrm{n,z}}|}}. \tag{D18}$$

To evaluate the influence of the coupling of nuclear spin, we define the non-dimension parameter by projection noise with coupling, i.e. $J \neq 0$ for $\delta B_{x,m}$, divided by projection noise without coupling, i.e. $J = 0$ for $\delta B_{x,m}$

$$\eta = \frac{\delta B_{x,m}|_{J\neq 0}}{\delta B_{x,m}|_{J=0}} \approx 1 + \frac{|D_0|}{|C_0|}. \tag{D19}$$

The approximation is satisfied when the coupling of nuclear spin and alkali atoms is weak, which is common experimental case for co-magnetometers operating at compensation point. We have also assumed that the distribution of nuclear spin is uniform corresponding to $m = 0$. When $\eta = 1$, it means that the coupling will not influence the projection noise of noble gas. When $\eta < 1$, it means that the coupling will reduce the projection noise of noble gas. When $\eta > 1$, it means that the coupling will promote the projection noise of noble gas. By setting $L = 5$ cm, $R = 0.3$ cm for vapor cell, $w_0 = 0.1$ cm for probe light, temperature $T = 463.15$ K, $|\bar{P}_{\mathrm{e},z}| = 0.95$ and $|\bar{P}_{\mathrm{n},z}| = 0.75$ [37], corresponding to $J = 30.53$ Hz, $\phi = 62.24$ and the result from previous modeling, we obtain $\eta = 1 + 0.13 > 1$ showing approximate 10% promotion for noble gas spin projection noise by coupling effect. This result is strongly dependent on temperature and we find a range for $1.10 \leqslant \eta \leqslant 1.18$ with the growth trend gradually slowing down when the temperature varying from 443.15 K to 523.15 K in the case above.

Appendix E. Eigenfunctions of the Helmholtz equation

Table 2. Eigenfunction and normalization coefficient at Dirichlet boundary condition(D-BC), Neumann boundary condition(N-BC), and Robin boundary condition(R-BC) in 3 common vapor cell shapes. J_n/j_l is the nth order Bessel/lth order spherical Bessel function and $k_{n\nu}/k_{ln}$ is the νth/nth eigen value for the nth order Bessel/lth order spherical Bessel function. $Y_{lm} = P_l^m(\cos\theta)\left\{\begin{array}{c}\sin m\phi\\ \cos m\phi\end{array}\right\}$ is spherical harmonics while $P_l^m(\cos\theta)$ is associated Lagendre function.

Cell Shape	Rectangle	Cylinder	Sphere
Axis Range	$0\leqslant x\leqslant a$ $0\leqslant y\leqslant b$ $0\leqslant z\leqslant c$	$0\leqslant \rho\leqslant R$ $0\leqslant \phi\leqslant 2\pi$ $0\leqslant z\leqslant L$	$0\leqslant r\leqslant R$ $0\leqslant \phi\leqslant 2\pi$ $0\leqslant \theta\leqslant \pi$
D-BC	$u_{nlm}(0,y,z)=u_{nlm}(a,y,z)=0$ $u_{nlm}(x,0,z)=u_{nlm}(x,b,z)=0$ $u_{nlm}(x,y,0)=u_{nlm}(x,y,c)=0$	$u_{n\nu lm}(R,\phi,z)=0, u_{n\nu lm}(0,\phi,z)\neq\infty$ $u_{n\nu lm}(r,\phi,z)=u_{n\nu lm}(r,\phi+2\pi,z)$ $u_{n\nu lm}(r,\phi,0)=u_{n\nu lm}(r,\phi,L)=0$	$u_{nlm}(R,\phi,\theta)=0, u_{nlm}(0,\phi,\theta)\neq 0$ $u_{nlm}(r,\phi,\theta)=u_{nlm}(r,\phi+2\pi,\theta)$ $u_{nlm}(r,\phi,0)\neq\infty$ $u_{nlm}(r,\phi,2\pi)\neq\infty$
Eigenfunction	$A_{nlm}\sin\frac{n\pi}{a}x\sin\frac{l\pi}{b}y\sin\frac{m\pi}{c}z$	$A_{n\nu lm}J_n(k_{n\nu}\rho)\sin\left(\frac{l\pi}{L}z\right)e^{im\phi}$	$A_{nlm}j_l(k_{ln}r)Y_{lm}(\theta,\phi)$
Normalization	$A_{nlm}=A_nA_lA_m$ $=\sqrt{\frac{2}{a}}\cdot\sqrt{\frac{2}{b}}\cdot\sqrt{\frac{2}{c}}$	$A_{n\nu lm}=A_{n\nu}A_lA_m$ $=\frac{\sqrt{2}}{R}\frac{1}{\lvert J_{n+1}(k_{n\nu}R)\rvert}\cdot\sqrt{\frac{2}{L}}\cdot A_m$ $A_m=\left\{\begin{array}{ll}\sqrt{\frac{1}{2\pi}} & m=0\\ 1 & m\neq 0\end{array}\right.$	$A_{nlm}=A_{ln}A_{lm}$ $=\sqrt{\frac{k_{ln}}{\pi R^2}}\frac{2}{J'_{l+\frac{1}{2}}(k_{ln}R)}\cdot\sqrt{\frac{2l+1}{2\pi\delta_m}\frac{(l-m)!}{(l+m)!}}$, $\delta_m=\left\{\begin{array}{ll}2 & ,m=0\\ 1 & ,m\neq 0\end{array}\right.$
N-BC	$u'_{nlm}(0,y,z)=u'_{nlm}(a,y,z)=0$ $u'_{nlm}(x,0,z)=u'_{nlm}(x,b,z)=0$ $u'_{nlm}(x,y,0)=u'_{nlm}(x,y,c)=0$	$u'_{n\nu lm}(R,\phi,z)=0, u_{n\nu lm}(0,\phi,z)\neq\infty$ $u_{n\nu lm}(r,\phi,z)=u_{n\nu lm}(r,\phi+2\pi,z)$ $u'_{n\nu lm}(r,\phi,0)=u'_{n\nu lm}(r,\phi,L)=0$	$u'_{nlm}(R,\phi,\theta)=0, u_{nlm}(0,\phi,\theta)\neq 0$ $u_{nlm}(r,\phi,\theta)=u_{nlm}(r,\phi+2\pi,\theta)$ $u_{nlm}(r,\phi,0)\neq\infty$ $u_{nlm}(r,\phi,2\pi)\neq\infty$
Eigenfunction	$A_{nlm}\cos\frac{n\pi}{a}x\cos\frac{l\pi}{b}y\cos\frac{m\pi}{c}z$	$A_{n\nu lm}J_n(k_{n\nu}\rho)\cos\left(\frac{l\pi}{L}z\right)e^{im\phi}$	$A_{nlm}j_l(k_{ln}r)Y_{lm}(\theta,\phi)$
Normalization	$A_{nlm}=A_nA_lA_m$ $=\sqrt{\frac{2}{a}}\cdot\sqrt{\frac{2}{b}}\cdot\sqrt{\frac{2}{c}}$	$A_{n\nu lm}=A_{n\nu}A_lA_m$ $=\sqrt{\frac{2}{R^2-\frac{n^2}{k_{n\nu}^2}}}\frac{1}{\lvert J_n(k_{n\nu}R)\rvert}\cdot\sqrt{\frac{2}{L}}\cdot A_m$ $A_m=\left\{\begin{array}{ll}\sqrt{\frac{1}{2\pi}} & m=0\\ 1 & m\neq 0\end{array}\right.$	$A_{nlm}=A_{ln}A_{lm}$ $=\sqrt{\frac{k_{ln}/\pi}{R^2-\frac{l(l+1)}{k_{ln}^2}}}\frac{2}{\left\lvert J_{l+\frac{1}{2}}(k_{ln}R)\right\rvert}\cdot$ $\sqrt{\frac{2l+1}{2\pi\delta_m}\frac{(l-m)!}{(l+m)!}}$, $\delta_m=\left\{\begin{array}{ll}2 & ,m=0\\ 1 & ,m\neq 0\end{array}\right.$
	$\alpha=\frac{2}{3}\frac{1+e^{-1/N}}{1-e^{-1/N}}\bar{\lambda}$		
R-BC	$u_{nlm}(0,y,z)+\alpha u'_{nlm}(0,y,z)=0$ $u_{nlm}(a,y,z)+\alpha u'_{nlm}(a,y,z)=0$ $u_{nlm}(x,0,z)+\alpha u'_{nlm}(x,0,z)=0$ $u_{nlm}(x,b,z)+\alpha u'_{nlm}(x,b,z)=0$ $u_{nlm}(x,y,0)+\alpha u'_{nlm}(x,y,0)=0$ $u_{nlm}(x,y,c)+\alpha u'_{nlm}(x,y,c)=0$	$u_{n\nu lm}(R,\phi,z)+\alpha u'_{n\nu lm}(R,\phi,z)=0$ $u_{n\nu lm}(0,\phi,z)\neq\infty$ $u_{n\nu lm}(r,\phi,z)=u_{n\nu lm}(r,\phi+2\pi,z)$ $u_{n\nu lm}(r,\phi,0)=u_{n\nu lm}(r,\phi,L)=0$	$u_{nlm}(R,\phi,\theta)+\alpha u'_{nlm}(R,\phi,\theta)=0$ $u_{nlm}(0,\phi,\theta)\neq 0$ $u_{nlm}(r,\phi,\theta)=u_{nlm}(r,\phi+2\pi,\theta)$ $u_{nlm}(r,\phi,0)\neq\infty$ $u_{nlm}(r,\phi,2\pi)\neq\infty$
Eigenfunction	$A_{nlm}(\sin k_nx-\alpha k_n\cos k_nx)\cdot$ $(\sin k_ly-\alpha k_l\cos k_ly)\cdot$ $(\sin k_mz-\alpha k_m\cos k_mz)$	$A_{n\nu lm}J_n(k_{n\nu}\rho)\cdot$ $(\sin k_lz+\cos k_lz)e^{im\phi}$	$A_{nlm}j_l(k_{ln}r)Y_{lm}(\theta,\phi)$
Normalization	$A_{nlm}=A_nA_lA_m$ $A_i=\sqrt{\frac{2/(1+\alpha^2k_n^2)}{L_i-B_i-C_i}}$ $B_i=\frac{\alpha(1+\cos 2k_nL_i)}{1+\alpha^2k_n^2}$ $C_i=\frac{1-\alpha^2k_n^2}{1+\alpha^2k_n^2}\frac{\sin 2k_nL_i}{2k_nL_i}$ $L_i=a,b,c$ $i=n,l,m$	$A_{n\nu lm}=A_{n\nu}A_lA_m$ $A_{n\nu}=\sqrt{\frac{2}{R^2-\frac{n^2}{k_{n\nu}^2}+\frac{R^2}{k_{n\nu}^2\alpha^2}}}\cdot$ $\frac{1}{\lvert J_n(k_{n\nu}R)\rvert}$ $A_l=\sqrt{\frac{2/(1+\alpha^2k_n^2)}{L-B-C}}$ $B=\frac{\alpha(1+\cos 2k_nL)}{1+\alpha^2k_n^2}$ $C=\frac{1-\alpha^2k_n^2}{1+\alpha^2k_n^2}\frac{\sin 2k_nL}{2k_nL}$ $A_m=\left\{\begin{array}{ll}\sqrt{\frac{1}{2\pi}} & m=0\\ 1 & m\neq 0\end{array}\right.$	$A_{nlm}=A_{ln}A_{lm}$ $A_{nl}=\sqrt{\frac{k_{ln}/\pi}{R^2+\frac{\frac{R}{\alpha}(\frac{R}{\alpha}-1)-l(l+1)}{k_{ln}^2}}}\cdot$ $\frac{2}{\left\lvert J_{l+\frac{1}{2}}(k_{ln}R)\right\rvert}$ $A_{lm}=\sqrt{\frac{2l+1}{2\pi\delta_m}\frac{(l-m)!}{(l+m)!}}$ $\delta_m=\left\{\begin{array}{ll}2 & ,m=0\\ 1 & ,m\neq 0\end{array}\right.$

References

[1] Degen C L, Reinhard F and Cappellaro P 2017 Quantum sensing *Rev. Mod. Phys.* **89** 035002
[2] Giovannetti V, Lloyd S and Maccone L 2011 Advances in quantum metrology *Nat. Photon.* **5** 222
[3] Pezzè L, Smerzi A, Oberthaler M K, Schmied R and Treutlein P 2018 Quantum metrology with nonclassical states of atomic ensembles *Rev. Mod. Phys.* **90** 035005

[4] Barbieri M 2022 Optical quantum metrology *PRX Quantum* **3** 010202
[5] Li H, Dou J-P, Pang X-L, Zhang C-N, Yan Z-Q, Yang T-H, Gao J, Li J-M and Jin X-M 2021 Multipartite entanglement of billions of motional atoms heralded by single photon *npj Quantum Inf.* **7** 146
[6] Zektzer R, Mazurski N, Barash Y and Levy U 2021 Nanoscale atomic suspended waveguides for improved vapour coherence times and optical frequency referencing *Nat. Photon.* **15** 772
[7] Lorenz V, Dai X, Green H, Asnicar T and Cundiff S 2008 High-density, high-temperature alkali vapor cell *Rev. Sci. Instrum.* **79** 123104
[8] Thaicharoen N, Moore K, Anderson D, Powel R, Peterson E and Raithel G 2019 Electromagnetically induced transparency, absorption and microwave-field sensing in a Rb vapor cell with a three-color all-infrared laser system *Phys. Rev.* A **100** 063427
[9] Griffith W C, Knappe S and Kitching J 2010 Femtotesla atomic magnetometry in a microfabricated vapor cell *Opt. Express* **18** 27167
[10] Chen Y, Quan W, Duan L, Lu Y, Jiang L and Fang J 2016 Spin-exchange collision mixing of the K and Rb ac stark shifts *Phys. Rev.* A **94** 052705
[11] Wei K, Zhao T, Fang X, Zhai Y, Li H and Quan W 2019 In-situ measurement of the density ratio of K-Rb hybrid vapor cell using spin-exchange collision mixing of the K and Rb light shifts *Opt. Express* **27** 16169
[12] Ito S, Ito Y and Kobayashi T 2019 Temperature characteristics of K-Rb hybrid optically pumped magnetometers with different density ratios *Opt. Express* **27** 8037
[13] Ding Y, Xiao W, Zhao Y, Wu T, Peng X and Guo H 2023 Dual-species all-optical magnetometer based on a Cs-K hybrid vapor cell *Phys. Rev. Appl.* **19** 034066
[14] Kornack T, Ghosh R and Romalis M V 2005 Nuclear spin gyroscope based on an atomic comagnetometer *Phys. Rev. Lett.* **95** 230801
[15] Brown J, Smullin S, Kornack T and Romalis M 2010 New limit on lorentz-and cpt-violating neutron spin interactions *Phys. Rev. Lett.* **105** 151604
[16] Quan W, Wei K, Zhao T, Li H and Zhai Y 2019 Synchronous measurement of inertial rotation and magnetic field using a K-Rb-^{21}Ne comagnetometer *Phys. Rev.* A **100** 012118
[17] Happer W and Tang H 1973 Spin-exchange shift and narrowing of magnetic resonance lines in optically pumped alkali vapors *Phys. Rev. Lett.* **31** 273
[18] Happer W and Tam A 1977 Effect of rapid spin exchange on the magnetic-resonance spectrum of alkali vapors *Phys. Rev.* A **16** 1877
[19] Appelt S, Baranga A B-A, Erickson C, Romalis M, Young A and Happer W 1998 Theory of spin-exchange optical pumping of ^{3}He and ^{129}Xe *Phys. Rev.* A **58** 1412
[20] Kadlecek S, Anderson L and Walker T 1998 Field dependence of spin relaxation in a dense Rb vapor *Phys. Rev. Lett.* **80** 5512
[21] Allred J, Lyman R, Kornack T and Romalis M V 2002 High-sensitivity atomic magnetometer unaffected by spin-exchange relaxation *Phys. Rev. Lett.* **89** 130801
[22] Kominis I, Kornack T, Allred J and Romalis M V 2003 A subfemtotesla multichannel atomic magnetometer *Nature* **422** 596
[23] Auzinsh M, Budker D, Kimball D, Rochester S, Stalnaker J, Sushkov A and Yashchuk V 2004 Can a quantum nondemolition measurement improve the sensitivity of an atomic magnetometer? *Phys. Rev. Lett.* **93** 173002
[24] Ledbetter M, Savukov I, Acosta V, Budker D and Romalis M 2008 Spin-exchange-relaxation-free magnetometry with Cs vapor *Phys. Rev.* A **77** 033408
[25] Wei K *et al* 2023 Ultrasensitive atomic comagnetometer with enhanced nuclear spin coherence *Phys. Rev. Lett.* **130** 063201
[26] Vasilakis G, Brown J, Kornack T and Romalis M 2009 Limits on new long range nuclear spin-dependent forces set with a K- He^3 comagnetometer *Phys. Rev. Lett.* **103** 261801
[27] Smiciklas M, Brown J, Cheuk L, Smullin S and Romalis M V 2011 New test of local lorentz invariance using a ^{21}Ne-Rb-K comagnetometer *Phys. Rev. Lett.* **107** 171604
[28] Limes M, Sheng D and Romalis M V 2018 ^{3}He–^{129}Xe comagnetometery using ^{87}Rb detection and decoupling *Phys. Rev. Lett.* **120** 033401
[29] Sheng D, Kabcenell A and Romalis M V 2014 New classes of systematic effects in gas spin comagnetometers *Phys. Rev. Lett.* **113** 163002
[30] Safronova M, Budker D, DeMille D, Kimball D F J, Derevianko A and Clark C W 2018 Search for new physics with atoms and molecules *Rev. Mod. Phys.* **90** 025008
[31] Jiang M, Su H, Garcon A, Peng X and Budker D 2021 Search for axion-like dark matter with spin-based amplifiers *Nat. Phys.* **17** 1402
[32] Ji W, Chen Y, Fu C, Ding M, Fang J, Xiao Z, Wei K and Yan H 2018 New experimental limits on exotic spin-spin-velocity-dependent interactions by using $smco_5$ spin sources *Phys. Rev. Lett.* **121** 261803
[33] Wei K, Ji W, Fu C, Wickenbrock A, Flambaum V V, Fang J and Budker D 2022 Constraints on exotic spin-velocity-dependent interactions *Nat. Commun.* **13** 7387
[34] Wasilewski W, Jensen K, Krauter H, Renema J J, Balabas M V and Polzik E S 2010 Erratum: Quantum noise limited and entanglement-assisted magnetometry *Phys. Rev. Lett.* **104** 209902
[35] Kong J, Jiménez-Martínez R, Troullinou C, Lucivero V G, Tóth G and Mitchell M W 2020 Measurement-induced, spatially-extended entanglement in a hot, strongly-interacting atomic system *Nat. Commun.* **11** 2415
[36] Shaham R, Katz O and Firstenberg O 2020 Quantum dynamics of collective spin states in a thermal gas *Phys. Rev.* A **102** 012822
[37] Katz O, Shaham R, Polzik E S and Firstenberg O 2020 Long-lived entanglement generation of nuclear spins using coherent light *Phys. Rev. Lett.* **124** 043602
[38] Li S, Vachaspati P, Sheng D, Dural N and Romalis M V 2011 Optical rotation in excess of 100 rad generated by Rb vapor in a multipass cell *Phys. Rev.* A **84** 061403
[39] Firstenberg O, London P, Yankelev D, Pugatch R, Shuker M and Davidson N 2010 Self-similar modes of coherent diffusion *Phys. Rev. Lett.* **105** 183602
[40] Xiao W, Wu T, Peng X and Guo H 2021 Atomic spin-exchange collisions in magnetic fields *Phys. Rev.* A **103** 043116
[41] Su H, Wang Y, Jiang M, Ji W, Fadeev P, Hu D, Peng X and Budker D 2021 Search for exotic spin-dependent interactions with a spin-based amplifier *Sci. Adv.* **7** eabi9535
[42] Yuchen J, Zhanchao L, Binquan Z, Xiaoyang L, Wenfeng W, Jinpeng P, Ming D, Yueyang Z and Jiancheng F 2019 Pump beam influence on spin polarization homogeneity in the nuclear magnetic resonance gyroscope *J. Phys. D: Appl. Phys.* **52** 355001
[43] Savukov I M, Seltzer S, Romalis M and Sauer K 2005 Tunable atomic magnetometer for detection of radio-frequency magnetic fields *Phys. Rev. Lett.* **95** 063004
[44] Romalis M and Cates G 1998 Accurate ^{3}He polarimetry using the Rb Zeeman frequency shift due to the Rb- ^{3}He spin-exchange collisions *Phys. Rev.* A **58** 3004

[45] Pei H, Duan L, Ma L, Fan S, Cai Z, Wu Z, Fan W and Quan W 2024 Real-time quantum control of spin-coupling damping and application in atomic spin gyroscopes *Cell Rep. Phys. Sci.* **5** 101832
[46] Wu Z, Pang H, Wang Z, Fan W, Liu F, Liu Y and Quan W 2024 A new design method for a triaxial magnetic field gradient compensation system based on ferromagnetic boundary *IEEE Trans. Ind. Electron.* 1–11
[47] Mcgregor D D 1990 Transverse relaxation of spin-polarized ^{3}He gas due to a magnetic field gradient *Phys. Rev.* A **41** 2631
[48] Dang H, Maloof A C and Romalis M V 2010 Ultrahigh sensitivity magnetic field and magnetization measurements with an atomic magnetometer *Appl. Phys. Lett.* **97** 151110
[49] Lucivero V, Lee W, Dural N and Romalis M 2021 Femtotesla direct magnetic gradiometer using a single multipass cell *Phys. Rev. Appl.* **15** 014004
[50] Almasi A, Lee J, Winarto H, Smiciklas M and Romalis M V 2020 New limits on anomalous spin-spin interactions *Phys. Rev. Lett.* **125** 201802
[51] Fadeev P, Stadnik Y V, Ficek F, Kozlov M G, Flambaum V V and Budker D 2019 Revisiting spin-dependent forces mediated by new bosons: potentials in the coordinate-space representation for macroscopic-and atomic-scale experiments *Phys. Rev.* A **99** 022113
[52] Jackson Kimball D F 2018 Spin gyroscope is ready to look for new physics *Physics* **11** 5
[53] Seltzer S J 2008 *Developments in Alkali-Metal Atomic Magnetometry* (Princeton University)
[54] Liu F, Duan L, Fan W, Pang H, Liu S, Wu J and Quan W 2021 Suppression method of light shift in K-Rb hybrid optical pumping serf atomic comagnetometer *IEEE Sens. J.* **21** 26665
[55] Zhao T, Wei K, Zhai Y and Tang C 2021 In-situ measurement of the density ratio of the K-Rb-^{21}Ne comagnetometer based on electron spin relaxation rate *J. Phys.: Conf. Ser.* **2112** 012010
[56] Seltzer S and Romalis M 2009 High-temperature alkali vapor cells with antirelaxation surface coatings *J. Appl. Phys.* **106** 114905
[57] Abel C *et al* 2019 Magnetic-field uniformity in neutron electric-dipole-moment experiments *Phys. Rev.* A **99** 042112
[58] Jackson J D 2021 *Classical Electrodynamics* 3rd edn (Wiley)
[59] Ghosh R K and Romalis M V 2010 Measurement of spin-exchange and relaxation parameters for polarizing ^{21}Ne with K and Rb *Phys. Rev.* A **81** 043415
[60] Kornack T W 2005 *A Test of CPT and Lorentz Symmetry Using a Potassium-Helium-3 co-Magnetometer* (Princeton University)
[61] Bevington P, Nicholson J, Zipfel J, Chalupczak W, Mishra C and Guarrera V 2024 Optical control and coherent coupling of spin diffusive modes in thermal gases (arXiv:2402.16750)
[62] Chang Y, Wan S, Dong S and Qin J 2024 Spin relaxation in inhomogeneous magnetic fields with depolarizing boundaries (arXiv:2403.08300)
[63] Katz O, Shaham R and Firstenberg O 2022 Quantum interface for noble-gas spins based on spin-exchange collisions *PRX Quantum* **3** 010305
[64] Kornack T W, Smullin S J, Lee S-K and Romalis M V 2007 A low-noise ferrite magnetic shield *Appl. Phys. Lett.* **90** 223501
[65] Lee S-K and Romalis M 2008 Calculation of magnetic field noise from high-permeability magnetic shields and conducting objects with simple geometry *J. Appl. Phys.* **103** 084904
[66] Julsgaard B, Sherson J, Cirac J I, Fiurášek J and Polzik E S 2004 Experimental demonstration of quantum memory for light *Nature* **432** 482
[67] Mouloudakis K *et al* 2023 Interspecies spin-noise correlations in hot atomic vapors *Phys. Rev.* A **108** 052822
[68] Mouloudakis K, Loulakis M and Kominis I 2019 Quantum trajectories in spin-exchange collisions reveal the nature of spin-noise correlations in multispecies alkali-metal vapors *Phys. Rev. Res.* **1** 033017
[69] Oswald R *et al* 2022 Search for dark-matter-induced oscillations of fundamental constants using molecular spectroscopy *Phys. Rev. Lett.* **129** 031302
[70] Tang Y, Liang C, Wen X, Li W, Xu A-N and Liu Y-C 2023 Pt-symmetric feedback induced linewidth narrowing *Phys. Rev. Lett.* **130** 193602
[71] Peng P, Cao W, Shen C, Qu W, Wen J, Jiang L and Xiao Y 2016 Anti-parity–time symmetry with flying atoms *Nat. Phys.* **12** 1139
[72] Zhang X, Hu J and Zhao N 2023 Stable atomic magnetometer in parity-time symmetry broken phase *Phys. Rev. Lett.* **130** 023201
[73] Happer W, Jau Y-Y and Walker T 2010 *Optically Pumped Atoms* (Wiley)